fer. Fractions containing IN were pooled and checked with SDS–PAGE.

4.3. CD spectroscopy of peptides with Glu-Lys substitution

CD measurements were performed on a JASCO J720 spectropolarimeter equipped with thermo-regulator (JASCO Corp., Ltd), using 5 μM of peptides dissolved in 0.1 M phosphate buffer, pH 5.6 containing 50% MeOH. UV spectra were recorded at 25 °C in a quartz cell 1.0 mm path length, a time constant of 1 s, and a 100 nm/min scanning speed with 0.1 nm resolution.

4.4. Integrase assays

Expression and purification of the recombinant IN in *E. coli* were performed as previously reported with addition of 10% glycerol to all buffers. Oigonucleotide substrates were prepared as described.[6] Integrase reactions were performed in 10 μL with 400 nM of recombinant IN, 20 nM of 5′-end [^{32}P]-labeled oligonucleotide substrate and inhibitors at various concentrations. Solutions of 10% DMSO without inhibitors were used as controls. Reaction mixtures were incubated at 37 °C (60 min) in buffer containing 50 mM MOPS, pH 7.2, 7.5 mM $MgCl_2$, and 14.3 mM 2-mercaptoethanol. Reactions were stopped by addition of 10 μL of loading dye (10 mM EDTA, 98% deionized formamide, 0.025% xylene cyanol and 0.025% bromophenol blue). Reactions were then subjected to electrophoresis in 20% polyacrylamide–7 M urea gels. Gels were dried and reaction products were visualized and quantitated with a Typhoon 8600 (GE Healthcare, Little Chalfont, Buckinghamshire, UK). Densitometric analyses were performed using ImageQuant from Molecular Dynamics Inc. The concentrations at which enzyme activity was reduced by 50% (IC_{50}) were determined using 'Prism' software (GraphPad Software, San Diego, CA) for nonlinear regression to fit dose–response data to logistic curve models.

4.5. Replication assays (MT-4 luciferase assays)

MT-4 luciferase cells (1×10^3 cells) grown in 96-well plates were infected with HIV-1_{HXB2} in the presence of various concentrations of peptides. At 6–7 days post-infection, cells were lysed and the luciferase activities were measured using the Steady-Glo assay kit (Promega), according to the manufacturer's protocol. Chemiluminescence was detected with a Veritas luminometer (Promega).

Acknowledgments

N.O. and T.T. are supported by JSPS research fellowships for young scientists. This work was supported by Mitsui Life Social Welfare Foundation, Grant-in-Aid for Scientific Research from the Ministry of Education, Culture, Sports, Science, and Technology of Japan, the Health and Labour Sciences Research Grants from Japanese Ministry of Health, Labor, and Welfare, and by the NIH Intramural Program, Center for Cancer Research, US National Cancer Institute.

Supplementary data

Supplementary data associated with this article can be found, in the online version, at doi:10.1016/j.bmc.2010.07.050.

References and notes

1. Mitsuya, H.; Erickson, J. In *Textbook of AIDS Medicine*; Merigan, T C., Bartlett, J. G., Bolognesi, D., Eds.; Williams & Wilkins: Baltimore, 1999; pp 751–780.
2. (a) Cahn, P.; Sued, O. *Lancet* **2007**, *369*, 1235; (b) Grinsztejn, B.; Nguyen, B.-Y.; Katlama, C.; Gatell, J. M.; Lazzarin, A.; Vittecoq, D.; Gonzalez, C. J.; Chen, J.; Harvey, C. M.; Isaacs, R. D. *Lancet* **2007**, *369*, 1261.
3. (a) Farnet, C. M.; Bushman, F. D. *Cell* **1997**, *88*, 483; (b) Chen, H.; Engelman, A. *Proc. Natl. Acad. Sci. U.S.A.* **1998**, *95*, 15270; (c) Gleenberg, I. O.; Herschhorn, A.; Hizi, A. *J. Mol. Biol.* **2007**, *369*, 1230; (d) Gleenberg, I. O.; Avidan, O.; Goldgur, Y.; Herschhorn, A.; Hizi, A. *J. Biol. Chem.* **2005**, *280*, 21987; (e) Hehl, E. A.; Joshi, P.; Kalpana, G. V.; Prasad, V. R. *J. Virol.* **2004**, *78*, 5056; (f) Tasara, T.; Maga, G.; Hottiger, M. O.; Hubscher, U. *FEBS Lett.* **2001**, *507*, 39; (g) Gleenberg, I. O.; Herschhorn, A.; Goldgur, Y.; Hizi, A. *Arch. Biochem. Biophys.* **2007**, *458*, 202.
4. Suzuki, S.; Urano, E.; Hashimoto, C.; Tsutsumi, H.; Nakahara, T.; Tanaka, T.; Nakanishi, Y.; Maddali, K.; Han, Y.; Hamatake, M.; Miyauchi, K.; Pommier, Y.; Beutler, J. A.; Sugiura, W.; Fuji, H.; Hoshino, T.; Itotani, K.; Nomura, W.; Narumi, T.; Yamamoto, N.; Komano, J. A.; Tamamura, H. *J. Med. Chem.* **2010**, *53*, 5356.
5. Suzuki, T.; Futaki, S.; Niwa, M.; Tanaka, S.; Ueda, K.; Sugiura, Y. *J. Biol. Chem.* **2002**, *277*, 2437.
6. (a) Yan, H.; Mizutani, T. C.; Nomura, N.; Tanaka, T.; Kitamura, Y.; Miura, H.; Nishizawa, M.; Tatsumi, M.; Yamamoto, N.; Sugiura, W. *Antivir. Chem. Chemother.* **2005**, *16*, 363; (b) Marchand, C.; Zhang, X.; Pais, G. C. G.; Cowansage, K.; Neamati, N.; Burke, T. R., Jr.; Pommier, Y. *J. Biol. Chem.* **2002**, *277*, 12596; (c) Semenova, E. A.; Johnson, A. A.; Marchand, C.; Davis, D. A.; Tarchoan, R.; Pommier, Y. *Mol. Pharmacol* **2006**, *69*, 1454; (d) Leh, H.; Brodin, P.; Bischerour, J.; Deprez, E.; Tauc, P.; Brochon, J. C.; LeCam, E.; Coulaud, D.; Auclair, C.; Mouscadet, J. F. *Biochemistry* **2000**, *39*, 9285; (e) Marchand, C.; Neamati, N.; Pommier, Y. In Vitro Human Immunodeficiency Virus Type 1 Integrase Assays. In *Methods in Enzymology (Drug-Nucleic Acid Interactions)*; Chaires, J. B., Waring, M. J., Eds.; Elsevier: Amsterdam, 2001; Vol. 340, pp 624–633.
7. Morellet, N.; Bouaziz, S.; Petitjean, P.; Roques, B. P. *J. Mol. Biol.* **2003**, *327*, 215.

Bioorganic & Medicinal Chemistry Letters 20 (2010) 5853–5858

Contents lists available at ScienceDirect

Bioorganic & Medicinal Chemistry Letters

journal homepage: www.elsevier.com/locate/bmcl

CD4 mimics targeting the HIV entry mechanism and their hybrid molecules with a CXCR4 antagonist

Tetsuo Narumi [a], Chihiro Ochiai [a], Kazuhisa Yoshimura [b], Shigeyoshi Harada [b], Tomohiro Tanaka [a], Wataru Nomura [a], Hiroshi Arai [a], Taro Ozaki [a], Nami Ohashi [a], Shuzo Matsushita [b], Hirokazu Tamamura [a,*]

[a] Institute of Biomaterials and Bioengineering, Tokyo Medical and Dental University, Chiyoda-ku, Tokyo 101-0062, Japan
[b] Center for AIDS Research, Kumamoto University, Kumamoto 860-0811, Japan

ARTICLE INFO

Article history:
Received 14 June 2010
Revised 22 July 2010
Accepted 26 July 2010
Available online 3 August 2010

Keywords:
CD4
HIV entry
Hybrid molecule
gp120

ABSTRACT

Small molecules behaving as CD4 mimics were previously reported as HIV-1 entry inhibitors that block the gp120–CD4 interaction and induce a conformational change in gp120, exposing its co-receptor-binding site. A structure–activity relationship (SAR) study of a series of CD4 mimic analogs was conducted to investigate the contribution from the piperidine moiety of CD4 mimic **1** to anti-HIV activity, cytotoxicity, and CD4 mimicry effects on conformational changes of gp120. In addition, several hybrid molecules based on conjugation of a CD4 mimic analog with a selective CXCR4 antagonist were also synthesized and their utility evaluated.

The infection of host cells by HIV-1 takes place in multiple steps via a dynamic supramolecular mechanism mediated by two viral envelope glycoproteins (gp41, gp120) and several cell surface proteins (CD4, CCR5/CXCR4).[1] Cell penetration begins with the interaction of gp120 with the primary receptor CD4. This induces conformational changes in gp120, leading to the exposure of its V3 loop allowing the subsequent binding of gp120 to a co-receptor, CCR5[2] or CXCR4.[3]

N-(4-Chlorophenyl)-*N'*-(2,2,6,6-tetramethyl-piperidin-4-yl)oxalamide (NBD-556: **1**) and the related compounds NBD-557 (**2**) and YYA-021 (**3**) have been identified as a novel class of HIV-1 entry inhibitors, which exert potent cell fusion and virus cell fusion inhibitory activity at low micromolar levels (Fig. 1).[4] Furthermore, compound **1** can also induce thermodynamically favored conformational changes in gp120 similar to those caused by CD4 binding. The X-ray crystal structure of gp120 complexed with CD4 revealed the presence of a hydrophobic cavity, the Phe43 cavity, which is penetrated by the aromatic ring of Phe^{43} of CD4.[5] Molecular modeling revealed that compound **1** is also inserted into the Phe43 cavity, the *para*-chlorophenyl group of **1** entering more deeply than the phenyl ring of Phe^{43} of CD4 and interacting with the conserved gp120 residues such as Trp^{427}, Phe^{382}, and Trp^{112}.[4c] The modeling also suggested that an oxalamide linker forms hydrogen bonds with carbonyl groups of the gp120 backbone peptide bonds. Our model of **1** docked into gp120 revealed that eight other gp120 residues, Val^{255}, Asp^{368}, Glu^{370}, Ser^{375}, Ile^{424}, Trp^{427}, Val^{430}, and Val^{475} are located within a 4.4 Å-radius of **1** and that a large cavity exists around the *p*-position of the aromatic ring of **1**.[4e] Based on these observations, we conducted a structure–activity relationship (SAR) study of a series of analogs of CD4 mimics with substituents at the *p*-position of the aromatic ring. This study revealed that a certain size and electron-withdrawing ability of the substituents are indispensable for potent anti-HIV activity.[4e]

Although several reported SAR studies of **1** have revealed the contributions of the phenyl ring and the oxalamide linker of **1** to the binding affinity with gp120, the anti-HIV activity and the CD4 mimicry on conformational changes of gp120,[4] there has been, to the best of our knowledge, no prior report describing SAR studies of the piperidine ring of **1**. In this paper, the contributions of the piperidine ring of **1** to the anti-HIV activity, CD4 mimicry and cytotoxicity were investigated through the SAR studies focused on the piperidine ring of **1**. Furthermore, to apply the utility of CD4 mimics to the development of potent anti-HIV agents, a series of the

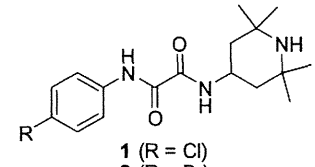

1 (R = Cl)
2 (R = Br)
3 (R = Me)

Figure 1. NBD-556 (**1**) and related compounds.

* Corresponding author.
E-mail address: tamamura.mr@tmd.ac.jp (H. Tamamura).

0960-894X/$ - see front matter © 2010 Elsevier Ltd. All rights reserved.
doi:10.1016/j.bmcl.2010.07.106

hybrid molecules that combined CD4 mimic analogs with a selective CXCR4 antagonist were also synthesized and bioevaluated.

For the design of novel CD4 mimic analogs, we initially tried to directly derivatize the nitrogen atom of piperidine group. However, direct alkylation and acylation of **1** failed probably as a result of steric hindrance from the methyl groups on the piperidine ring so we synthesized several derivatives lacking the methyl groups and evaluated their anti-HIV activity, cytotoxicity, and ability to mimic CD4. According to the previous SAR study,[4e] the *p*-Cl (**4**), *p*-Br (**5**) and *p*-methyl derivatives (**6**) lacking the methyl groups on the piperidine ring were prepared. Compounds **4–6** were synthesized by published methods as shown in Scheme 1. Briefly, coupling of aniline derivatives with ethyl chloroglyoxalate in the presence of Et_3N and subsequent saponification gave the corresponding acids (**10–12**). Condensation of these acids with 4-amino-*N*-benzylpiperidine in the presence of EDC–HOBt system, followed by debenzylation under von Braun conditions with 1-chloroethyl choroformate[6] produced the desired compounds **4–6**.[7]

The anti-HIV activity of each of the synthetic compounds was evaluated against MNA (R5) strain, with the results shown in Table 1. IC_{50} values were determined by the 3-(4,5-dimethylthiazol-2-yl)-2,5-diphenyltetrazolium bromide (MTT) method[8] as the concentrations of the compounds which conferred 50% protection against HIV-1-induced cytopathogenicity in PM1/CCR5 cells. Cytotoxicity of the compounds based on the viability of mock-infected PM1/CCR5 cells was also evaluated using the MTT method. CC_{50} values, the concentrations achieving 50% reduction of the viability of mock-infected cells, were also determined. Compounds **1** and **3** showed potent anti-HIV activity. The anti-HIV IC_{50} of compound **2** was previously reported to be comparable to that of compound **1**, and thus was not determined in this study. Novel derivatives **4** and **6** without the methyl groups on the piperidine ring, showed significant anti-HIV activity comparable to that of the parent compounds **1** and **3**, respectively. The *p*-methyl derivative **6** has slightly lower activity than the *p*-Cl derivative **4** and the *p*-Br derivative **5**. These results are consistent with our previous SAR studies on the parent compounds **1–3**. Compound **5** was found to exhibit relatively strong cytotoxicity (CC_{50} = 50 μM) and compounds **4** and **6** have cytotoxicities comparable to that of compounds **1** and **3**, respectively. This observation indicates that the methyl groups on the piperidine ring do not contribute significantly to the anti-HIV activity or the cytotoxicity.

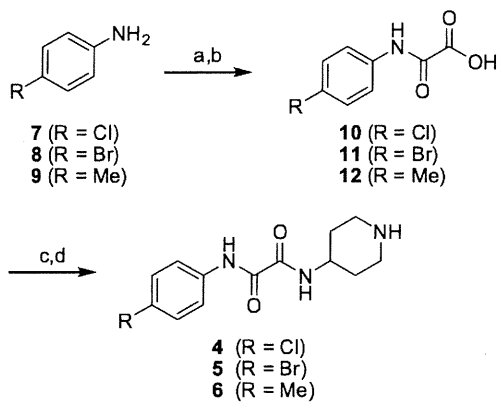

Scheme 1. Synthesis of compounds **4–6**. Reagents and conditions: (a) ethyl chloroglyoxylate, Et_3N, THF; (b) 1 M aq NaOH, THF, 67%–quant.; (c) 1-benzyl-4-aminopiperidine, EDC·HCl, HOBt·H_2O, Et_3N, THF; (d) (i) 1-chloroethyl chloroformate, CH_2Cl_2; (ii) MeOH, 8–47%.

Table 1
Effects of the methyl groups on anti-HIV activity and cytotoxicity of CD4 mimic analogs[a]

Compd	R	IC_{50} (μM) MNA (R5)	CC_{50} (μM)
1	Cl	12	110
2	Br	ND	93
3	Me	15	210
4	Cl	8	100
5	Br	6	50
6	Me	20	190

[a] All data with standard deviation are the mean values for at least three independent experiments (ND = not determined).

Compound **1** and the newly synthesized derivatives **4–6** were also evaluated for their effects on conformational changes of gp120 by a fluorescence activated cell sorting (FACS) analysis. The profile of binding of an anti-envelope CD4-induced monoclonal antibody (4C11) to the Env-expressing cell surface (an R5-HIV-1 strain, JR-FL, -infected PM1 cells) pretreated with the above derivatives was examined. Comparison of the binding of 4C11 to the cell surface was measured in terms of the mean fluorescence intensity (MFI), as shown in Figure 2. Pretreatment of the Env-expressing cell surface with compound **1** (MFI = 53.66) produced a significant increase in binding affinity for 4C11, consistent with that reported previously.[4e] This indicates that compound **1** enhances the binding affinity of gp120 with the 17b monoclonal antibody which recognizes CD4-induced epitopes on gp120. The Env-expressing cells without CD4 mimic-pretreatment failed to show significant binding affinity to 4C11. On the other hand, the profiles of the binding of 4C11 to the Env-expressing cell surface pretreated with compound **4** (Cl derivative) and **5** (Br derivative) (MFI = 49.88 and 52.34) were similar to that of compound **1**. Pretreatment of the cell surface with compound **6** (Me derivative) (MFI = 45.99) produced slightly lower enhancement but significant levels of binding affinity for 4C11, compared to that of compound **1** as pretreatments. These results suggested that the removal of the methyl groups on the piperidine moiety might not affect the CD4 mimicry effects on conformational changes of gp120 and it was conjectured that the phenyl ring of CD4 mimic might be a key moiety for the interaction with gp120 to induce the conformational changes of gp120. This is consistent with the results in the previous paper where it was reported that CD4 mimics having suitable substituent(s) on the phenyl ring cause a conformational change, resulting in external exposure of the co-receptor-binding site of gp120.[4e]

Based on these results, a series of N-alkylated and N-acylated piperidine derivatives **13–18** with no methyl groups were prepared. Several compounds with 6-membered rings were also prepared to determine whether or not the piperidine ring is mandatory. The synthesis of these derivatives is shown in Scheme 2. Since the *p*-Cl derivative **4** showed potent anti-HIV activity and relatively low cytotoxicity, compared to the *p*-Br derivative **5**, chlorine was selected as the substituent at the *p*-position of the phenyl ring. The N-methyl derivative **13** was synthesized by coupling of **10** with 4-amine-1-methylpiperidine. Alkylation of **4** with *tert*-butyl bromoacetate, followed by deprotection of *tert*-butyl ester provided compound **14**. The N-isopropyl derivative **15** was prepared by reductive amination of **4** with isopropyl aldehyde. The N-acyl derivatives **16–18** were prepared by simple acylation or condensation with the corresponding substrate. The synthesis of other derivatives **19–23** with different 6-membered rings is depicted in Scheme 3. The 6-membered ring derivatives with the exception of **21** were prepared by coupling of acid **10** with the corresponding amines. Compound **21** was prepared by reaction of **10** with thionyl chloride to give the corresponding acid chloride, which was subsequently coupled with 4-aminopyridine.

Compounds **1**, **3**, and **13–18** were evaluated for their CD4 mimicry effects on conformational changes of gp120 by the FACS anal-

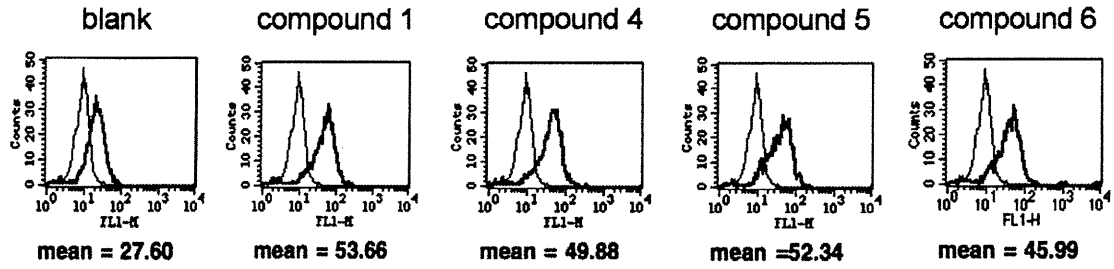

Figure 2. FACS analysis of compounds **1** and **4–6**. JR-FL (R5, Sub B) chronically infected PM1 cells were preincubated with 100 μM of a CD4 mimic for 15 min, and then incubated with an anti-HIV-1 mAb, 4C11, at 4 °C for 15 min. The cells were washed with PBS, and fluorescein isothiocyanate (FITC)-conjugated goat anti-human IgG antibody was used for antibody-staining. Flow cytometry data for the binding of 4C11 (green lines) to the Env-expressing cell surface in the presence of a CD4 mimic are shown among gated PM1 cells along with a control antibody (anti-human CD19:black lines). Data are representative of the results from a minimum of two independent experiments. The number at the bottom of each graph shows the mean fluorescence intensity (MFI) of the antibody 4C11.

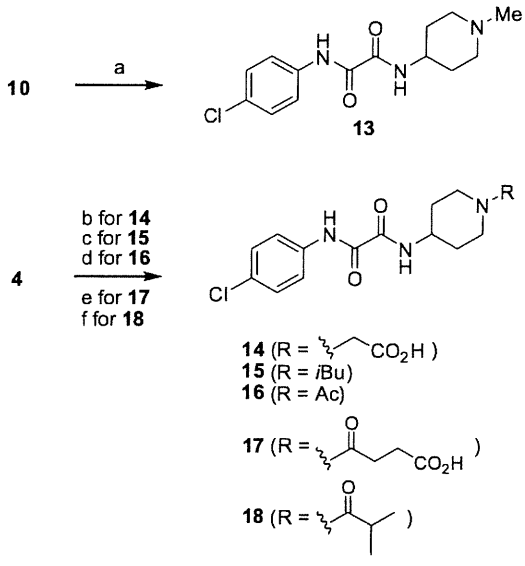

Scheme 2. Synthesis of N-alkylated and N-acylated piperidine derivatives **13–18**. Reagents and conditions: (a) 4-amine-1-methylpiperidine, EDC·HCl, HOBt·H_2O, Et_3N, THF, 16%; (b) (i) *tert*-butyl bromoacetate, NaH, DMF; (ii) TFA, 6%; (c) isobutylaldehyde, $NaBH(OAc)_3$, AcOH, DCE, quant.; (d) acetyl chloride, Et_3N, DMF, quant.; (e) succinic anhydride, Et_3N, THF, 37%; (f) isobutyric acid, EDC·HCl, HOBt·H_2O, Et_3N, THF, 95%.

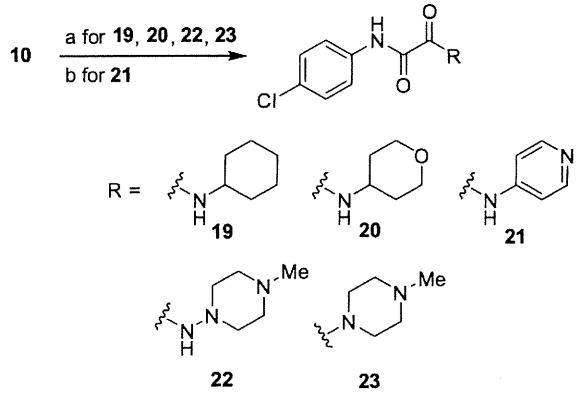

Scheme 3. Synthesis of 6-membered ring derivatives **19–23**. Reagents and conditions: (a) the corresponding amine, EDC·HCl, HOBt·H_2O, Et_3N, THF, 22%–quant.; (b) 4-aminopyridine, $SOCl_2$, MeOH, 38%.

ysis, and the results are shown in Figure 3. Pretreatment of the Env-expressing cells with the N-substituted compounds **13**, **15**, **16**, and **18** produced a notable increase in binding affinity to 4C11, similar to that observed in the pretreatment with compound **1**. The profile of the binding of 4C11 to the cell surface pretreated with compounds **14** and **17** was similar to that of controls, suggesting that these derivatives offer no significant enhancement of binding affinity for 4C11 and that the carboxylic moiety in the terminal of piperidine ring is not suited to CD4 mimicry. It is hypothesized that the carboxylic moieties of compounds **14** and **17** might prevent the interaction of CD4 mimic with gp120 by their multiple contacts with side chain(s) of amino acid(s) around the Phe43 cavity, such as Asp^{368} and Glu^{370}. Replacement of the piperidine moiety with the different 6-membered rings resulted in a significant loss of binding affinity for 4C11 in the FACS analysis of compound **19–23** (MFI(**19**) = 11.44, MFI(**20**) = 12.84, MFI(**21**) = 12.47, in MFI (blank) = 11.34; MFI(**22**) = 26.67, MFI(**23**) = 20.21, in MFI(blank) = 26.79, data not shown), indicating a significant contribution from the piperidine ring which interacts with gp120 inducing conformational changes.

In view of their ability to induce conformational changes of gp120, the anti-HIV activity and cytotoxicity of the piperidine derivatives **13–18** were further evaluated, with the results shown in Table 2. The anti-HIV activity of the synthetic compounds was evaluated against various viral strains including both laboratory and primary isolates and IC_{50} and CC_{50} values were determined as those of compounds **4–6**. The *N*-methylpiperidine compound **13**, was not found to possess significant anti-HIV activity against a primary isolate, but was found to possess moderate anti-HIV activity against a laboratory isolate, a IIIB strain (IC_{50} = 67 μM). Anti-HIV activity was not observed however, even at concentrations of 100 μM of **13** against an 89.6 strain. The potency was approximately eight-fold lower than that of the parent compound **1** (IC_{50} = 8 μM), indicating a partial contribution of the hydrogen atom of the amino group of the piperidine ring to the bioactivity of CD4 mimic. Although compound **15**, with an *N*-isobutylpiperidine moiety, failed to show significant anti-HIV activity against laboratory isolates, relativity potent activity was observed against a primary isolate, an MTA strain (IC_{50} = 28 μM). Compounds **16** and **18**, which are *N*-acylpiperidines, were tested against laboratory isolates and significant anti-HIV activity was not observed even at 100 μM. Compounds **14** and **17**, with the carboxylic moieties, failed to show significant anti-HIV activity against laboratory isolates even at 100 μM, which are compatible with the FACS analysis. These results suggest that the N-substituent on the piperidine ring of CD4 mimic analogs may contribute to a critical interaction required for binding to gp120. Compounds **19–23** showed no significant anti-HIV activity against a IIIB strain even at 100 μM, which are compatible with the FACS analysis (data not shown).

All but one of the compounds **13–18** have no significant cytotoxicity to PM1/CCR5 cells ($CC_{50} \geqslant 260$ μM); the exception is compound **18** (CC_{50} = 45 μM). Compounds **13** and **15** show relatively potent anti-HIV activity without significant cytotoxicity.

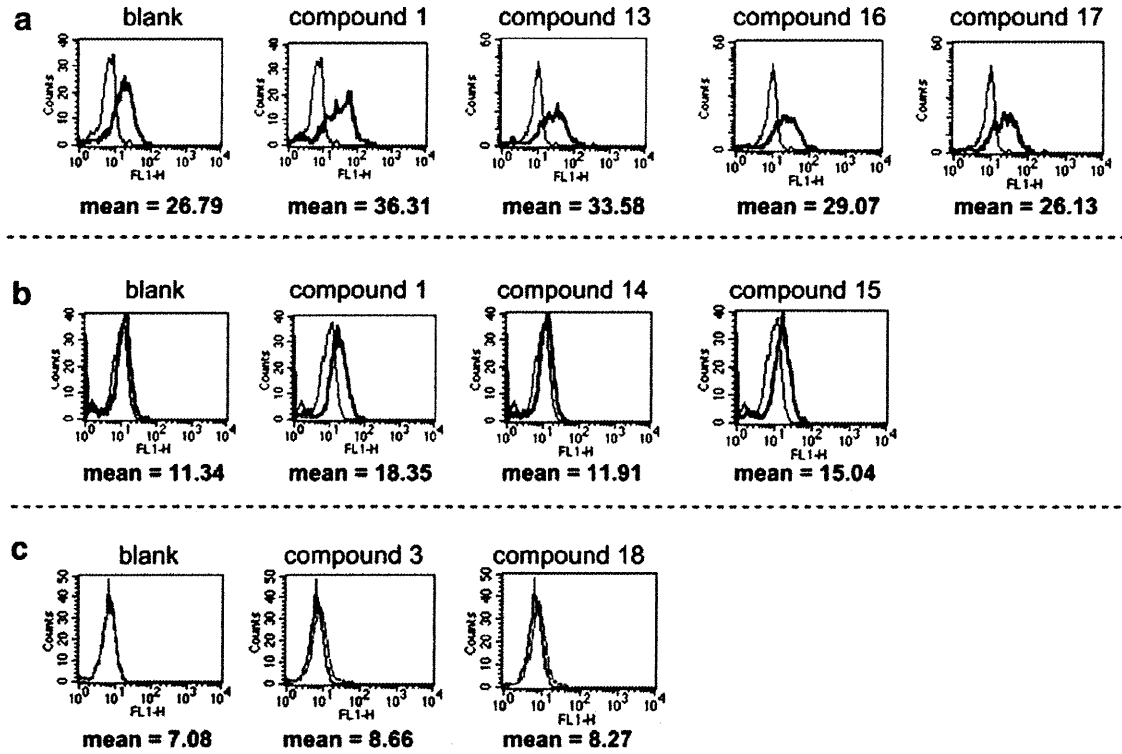

Figure 3. FACS analysis of compounds **1**, **3**, and **13–18**. The experimental procedures are described in Figure 2. The lanes of (a), (b) and (c) show independent experiments.

Table 2
Anti-HIV activity and cytotoxicity of compounds **13–18**[a]

Compd	R	IC_{50} (μM)			CC_{50} (μM)
		Laboratory isolates		Primary isolates	
		IIIB (X4)	89.6 (dual)	MTA (R5)	
1		8	10	ND	150
4	H	ND	ND	ND	100
13	Me	67	>100	ND	>300
14	CH_2CO_2H	>100	ND	ND	260
15	*i*Bu	>100	ND	28	>300
16	Ac	>100	>100	ND	>300
17	$C(O)CH_2CH_2CO_2H$	>100	>100	ND	>300
18	C(O)*i*Pr	>100	ND	ND	45

[a] All data with standard deviation are the mean values for at least three independent experiments.

The results for **15** showed it to have 3–6 times less cytotoxicity than **4** and **18**. This observation indicates that the alkylation of the piperidine nitrogen may be favorable because it lowers the cytotoxicity of CD4 mimic analogs.

In the course of the SAR studies on CD4 mimic analogs, we have already found that a CD4 mimic or sCD4 exhibited a remarkable synergistic effect[4e] with a 14-mer peptide CXCR4 antagonist T140.[9] This result indicates that the interaction of CD4 mimic with gp120 could facilitate the approach of CXCR4 to gp120 by exposing the co-receptor binding site of gp120. It was thought that the CD4 mimic analogs conjugated with a selective CXCR4 antagonist might as a consequence show a higher synergistic effect for the improvement of anti-HIV activity. In this context, efforts were made to synthesize and bioevaluate hybrid molecules that combined a CD4 mimic analog with 4F-benzoyl-TZ14011, which is a derivative of T140 optimized for CXCR4 binding and stability in vivo.[10]

The synthesis of hybrid molecules **27–29** is outlined in Scheme 4. To examine the influence of the linker length on anti-HIV activity and cytotoxicity, three hybrid molecules with linkers of different lengths were designed. Based on the fact that alkylation of the piperidine nitrogen, having no deleterious effects on bioactivity, is an acceptable modification of CD4 mimic analogs, the alkylamine moiety was incorporated into the nitrogen atom of the piperidine moiety to conjugate CD4 mimic analogs with 4F-benzoyl-TZ14011. Reductive alkylation of **4** with N^{α}-Boc-pyrrolidin-2-ol **24**, which exists in equilibrium with the corresponding aldehyde, and successive treatment with TFA and HCl/dioxane provided the amine hydrochloride **25**. Treatment of **25** with succinic anhydride under basic condition gave the corresponding acid **26**, which was subjected to condensation with the side chain of D-Lys[8] of 4F-benzoyl-TZ14011 in an EDC–HOBt system to give the desired hybrid molecule **27** with a tetramethylene linker.[11] Other hybrid molecules **28** and **29** bearing hexa- and octamethylene linkers, respectively, were prepared using the corresponding aldehydes **30** and **31**.

The assay results for these hybrid molecules **27–29** are shown in Table 3. To investigate the effect of conjugation of two molecules on binding activity against CXCR4, the inhibitory potency against

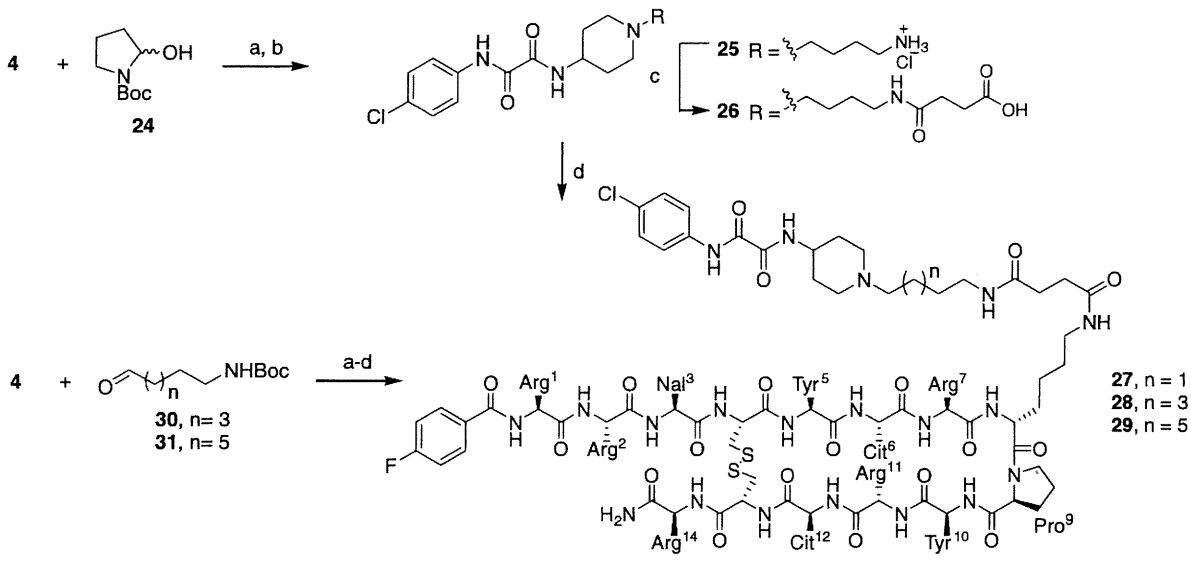

Scheme 4. Synthesis of hybrid molecules **27–29**. Reagents and conditions: (a) $NaBH(OAc)_3$, AcOH, DCE; (b) TFA, then 4 M HCl/1,4-dioxane; (c) succinic anhydride, pyridine, DMF, then 4 M HCl/1,4-dioxane; (d) 4F-benzoyl-TZ14011, EDC·HCl, HOBt·H_2O, Et_3N, DMF. Nal = L-3-(2-naphthyl)alanine, Cit = L-citrulline.

Table 3
CXCR4-binding activity, anti-HIV activity and cytotoxicity of hybrid molecules **27–29**[a]

Compd	EC_{50}[b] (μM)	IC_{50}[c] (μM)	CC_{50}[d] (μM)	SI (CC_{50}/IC_{50})
4F-benzoyl-TZ14011	0.0059	0.0131	ND	ND
1 (NBD-556)	ND	0 2.10	ND	19.2[e]
27 (C4)	0.0044	0.0509	8.60	169
28 (C6)	0.0187	0.0365	8.00	219
29 (C8)	0.0071	0.0353	8.60	244
AZT	ND	0.0493	ND	ND

[a] All data with standard deviation are the mean values for at least three independent experiments.
[b] EC_{50} values are based on the inhibition of [^{125}I]-SDF-1α binding to CXCR4 transfectants of CHO cells.
[c] IC_{50} values are based on the inhibition of HIV-1-induced cytopathogenicity in MT-2 cells.
[d] CC_{50} values are based on the reduction of the viability of mock-infected MT-2 cells.
[e] This value is based on the CC_{50} and IC_{50} values from Table 1.

binding of [^{125}I]-SDF-1α to CXCR4 was measured. All the hybrid molecules **27–29** significantly inhibited the SDF-1α binding to CXCR4. The corresponding EC_{50} values are: EC_{50}(**27**) = 0.0044 μM; EC_{50}(**28**) = 0.0187 μM; EC_{50}(**29**) = 0.0071 μM. These potencies are comparable to that of 4F-benzoyl-TZ14011 (EC_{50} = 0.0059 μM), indicating that introduction of the CD4 mimic analog into the D-Lys^8 residue of 4F-benzoyl-TZ14011 does not affect binding activity against CXCR4. Comparison of the binding activities of **27–29** showed that all hybrid molecules were essentially equipotent in inhibition of the binding of SDF-1α to CXCR4. This observation indicates that the linker length between two molecules has no effect on the binding inhibition.

Anti-HIV activity based on the inhibition of HIV-1 entry into the target cells was examined by the MTT assay using a IIIB(X4) strain. In this assay, the IC_{50} value of 4F-benzoyl-TZ14011 was 0.0131 μM. All hybrid molecules **27–29** showed significant anti-HIV activity [IC_{50}(**27**) = 0.0509 μM; IC_{50}(**28**) = 0.0365 μM; IC_{50}(**29**) = 0.0353 μM]; however, the potency was 2- to 4-fold lower than that of the parent compound 4F-benzoyl-TZ14011, indicating that the conjugation of CD4 mimic with a CXCR4 antagonist did not provide a significant synergistic effect. In view of the fact that the combinational uses of CD4 mimic with T140 produced a highly remarkable synergistic effect, the lower potency of hybrid molecules may be attributed to the inadequacy in the structure and/or the characters of the linkers. All the hybrid molecules **27–29** have relatively strong cytotoxicity [CC_{50}(**27**) = 8.6 μM; CC_{50}(**28**) = 8.0 μM; CC_{50}(**29**) = 8.6 μM]. However, selectivity indexes (SI = CC_{50}/IC_{50}) were 169 for **27**, 219 for **28**, and 244 for **29**, all 9–13 times higher than that of **1** (SI = 9.2). This result indicates that conjugation of a CD4 mimic analog with a selective CXCR4 antagonist can improve the SI of CD4 mimic.

The SAR study of a series of CD4 mimic analogs was conducted to investigate the contribution of the piperidine moiety of **1** to anti-HIV activity, cytotoxicity, and CD4 mimicry on conformational changes of gp120. The results indicate that (i) the methyl groups on the piperidine ring of **1** have no great influence on the activities of CD4 mimic; (ii) the presence of piperidine moiety is important for the CD4 mimicry; and (iii) N-substituents of the piperidine moiety contribute significantly to anti-HIV activity and cytotoxicity, as observed with N-alkyl groups such as methyl and isobutyl groups which show moderate anti-HIV activity and lower cytotoxicity.

Several hybrid molecules based on conjugation of a CD4 mimic with a selective CXCR4 antagonist were also synthesized and bioevaluated. All the hybrid molecules showed significant binding activity against CXCR4 comparable to the parent antagonist and exhibited potent anti-HIV activity. Although no significant synergistic effect was observed, conjugation of a CD4 mimic with a selective CXCR4 antagonist might lead to the development of novel type of CD4 mimic-based HIV-1 entry inhibitors, which possess higher selective indexes than a simple CD4 mimic. These results will be useful for the rational design and synthesis of a new type of HIV-1 entry inhibitors. Further structural modification studies of CD4 mimic are the subject of an ongoing project.

Acknowledgements

This work was supported by Grant-in-Aid for Scientific Research from the Ministry of Education, Culture, Sports, Science, and Technology of Japan, Japan Human Science Foundation, and Health and Labour Sciences Research Grants from Japanese Ministry of Health, Labor, and Welfare. T.T. and N.O. are grateful for the JSPS Reseach Fellowships for Young Scientist.

References and notes

1. Chan, D. C.; Kim, P. S. *Cell* **1998**, *93*, 681.
2. (a) Alkhatib, G.; Combadiere, C.; Broder, C. C.; Feng, Y.; Kennedy, P. E.; Murphy, P. M.; Berger, E. A. *Science* **1996**, *272*, 1955; (b) Choe, H.; Farzan, M.; Sun, Y.; Sullivan, N.; Rollins, B.; Ponath, P. D.; Wu, L.; Mackay, C. R.; LaRosa, G.; Newman, W.; Gerard, N.; Gerard, C.; Sodroski, J. *Cell* **1996**, *85*, 1135; (c) Deng, H. K.; Liu, R.; Ellmeier, W.; Choe, S.; Unutmaz, D.; Burkhart, M.; Marzio, P. D.; Marmon, S.; Sutton, R. E.; Hill, C. M.; Davis, C. B.; Peiper, S. C.; Schall, T. J.; Littman, D. R.; Landau, N. R. *Nature* **1996**, *381*, 661; (d) Doranz, B. J.; Rucker, J.; Yi, Y. J.; Smyth, R. J.; Samson, M.; Peiper, S. C.; Parmentier, M.; Collman, R. G.; Doms, R. W. *Cell* **1996**, *85*, 1149; (e) Dragic, T.; Litwin, V.; Allaway, G. P.; Martin, S. R.; Huang, Y.; Nagashima, K. A.; Cayanan, C.; Maddon, P. J.; Koup, R. A.; Moore, J. P.; Paxton, W. A. *Nature* **1996**, *381*, 667.
3. Feng, Y.; Broder, C. C.; Kennedy, P. E.; Berger, E. A. *Science* **1996**, *272*, 872.
4. (a) Zhao, Q.; Ma, L.; Jiang, S.; Lu, H.; Liu, S.; He, Y.; Strick, N.; Neamati, N.; Debnath, A. K. *Virology* **2005**, *339*, 213; (b) Schön, A.; Madani, N.; Klein, J. C.; Hubicki, A.; Ng, D.; Yang, X.; Smith, A. B., III; Sodroski, J.; Freire, E. *Biochemistry* **2006**, *45*, 10973; (c) Madani, N.; Schön, A.; Princiotto, A. M.; LaLonde, J. M.; Courter, J. R.; Soeta, T.; Ng, D.; Wang, L.; Brower, E. T.; Xiang, S.-H.; Do Kwon, Y.; Huang, C.-C.; Wyatt, R.; Kwong, P. D.; Freire, E.; Smith, A. B., III; Sodroski, J. *Structure* **2008**, *16*, 1689; (d) Haim, H.; Si, Z.; Madani, N.; Wang, L.; Courter, J. R.; Princiotto, A.; Kassa, A.; DeGrace, M.; McGee-Estrada, K.; Mefford, M.; Gabuzda, D., ; Smith, A. B., III; Sodroski, J. *ProS Pathogens* **2009**, *5*, 1; (e) Yamada, Y.; Ochiai, C.; Yoshimura, K.; Tanaka, T.; Ohashi, N.; Narumi, T.; Nomura, W.; Harada, S.; Matsushita, S.; Tamamura, H. *Bioorg. Med. Chem. Lett.* **2010**, *20*, 354; (f) Yoshimura, K.; Harada, S.; Shibata, J.; Hatada, M.; Yamada, Y.; Ochiai, C.; Tamamura, H.; Matsushita, S. *J. Virol.* **2010**, *84*, 7558.
5. Protein Data Bank (PDB) (entry 1RZJ).
6. Olofson, R. A.; Abbott, D. E. *J. Org. Chem.* **1984**, *49*, 2795.
7. The synthesis of compound **4**: To the solution of compound **10** (104 mg, 0.52 mmol) in dry THF (4.0 mL), Et_3N (159 μL, 1.15 mmol), HOBt·H_2O (87 mg, 0.57 mmol), EDCI·HCl (109 mg, 0.57 mmol) and 4-amino-1-benzylpiperidine (109 μL, 0.57 mmol) were added with stirring at 0 °C, and continuously stirred for 6 h with warming to room temperature under N_2 atmosphere. After concentration under reduced pressure, the residue was extracted with EtOAc. The extract was washed with aq saturated $NaHCO_3$ and brine, and dried over $MgSO_4$. Concentration under reduced pressure followed by flash chromatography over silica gel with $CHCl_3$–MeOH (20:1) including 1% Et_3N gave the crude benzyl amine as a white powder. To the solution of the above crude benzyl amine (95 mg, 0.26 mmol) in dry CH_2Cl_2 (10 mL), 1-chloroethyl chloroformate (110 μL, 0.68 mmol) was added dropwise with stirring at 0 °C. The mixture was then refluxed for 3 h under N_2 atmosphere. After concentration under reduced pressure, the residue was resolved in MeOH (10 mL) and then refluxed for 1 h. Concentration under reduced pressure gave a crude product. Reprecipitation with MeOH–Et_2O afforded a white powder of the title compound **4** (33 mg, 46% yield). δ_H(400 MHz; CD_3OD) 1.83–1.92 (2H, m, CH_2), 2.10–2.17 (2H, m, CH_2), 3.13 (2H, t, *J* 12.5, CH_2), 3.34 (1H, m, NH), 3.42–3.49 (1H, m, CH_2), 4.04 (1H, m, CH), 7.34 (2H, m, ArH), 7.51 (1H, m, NH), 7.73 (2H, m, ArH), 8.84 (1H, m, NH); LRMS (ESI), *m/z* calcd for $C_{13}H_{17}ClN_3O_2$ $(MH)^+$ 282.10, found 282.14.
8. Yoshimura, K.; Shibata, J.; Kimura, T.; Honda, A.; Maeda, Y.; Koito, A.; Murakami, T.; Mitsuya, H.; Matsushita, S. *AIDS* **2006**, *20*, 2065.
9. (a) Tamamura, H.; Xu, Y.; Hattori, T.; Zhang, X.; Arakaki, R.; Kanbara, K.; Omagari, A.; Otaka, A.; Ibuka, T.; Yamamoto, N.; Nakashima, H.; Fujii, N. *Biochem. Biophys. Res. Commun.* **1998**, *253*, 877; (b) Tamamura, H.; Hiramatsu, K.; Mizumoto, M.; Ueda, S.; Kusano, S.; Terakubo, S.; Akamatsu, M.; Yamamoto, N.; Trent, J. O.; Wang, Z.; Peiper, S. C.; Nakashima, H.; Otaka, A.; Fujii, N. *Org. Biomol. Chem.* **2003**, *1*, 3663.
10. Hanaoka, H.; Mukai, T.; Tamamura, H.; Mori, T.; Ishino, S.; Ogawa, K.; Iida, Y.; Doi, R.; Fujii, N.; Saji, H. *Nucl. Med. Biol.* **2006**, *33*, 489.
11. The synthesis of a hybrid molecule **27**: To the solution of compound **26** (2.6 mg, 4.6 μmol) in DMF (1.0 mL), Et_3N (26 μL, 92 μmol), HOBt·H_2O (3.5 mg, 23 μmol) and EDCI·HCl (4.5 mg, 23 μmol) were added with stirring at 0 °C, and stirred for 1 h at room temperature. To the mixture 4F-benzoyl-TZ14011 (15 mg, 4.1 μmol) was then added and the mixture was stirred for 24 h at room temperature under N_2 atmosphere. After concentration under reduced pressure, the residue was purified by reversed phase HPLC (t_R = 23 min, elution: a linear gradient of 27–31% acetonitrile containing 0.1% TFA over 30 min) to afford a fluffy white powder of the desired compound **27** (1.3 mg, 9.8%). LRMS (ESI), *m/z* 2621.20 $[M+H]^+$, calcd 2620.25.

J|A|C|S COMMUNICATIONS

Published on Web 10/25/2010

Bivalent Ligands of CXCR4 with Rigid Linkers for Elucidation of the Dimerization State in Cells

Tomohiro Tanaka, Wataru Nomura,* Tetsuo Narumi, Akemi Masuda, and Hirokazu Tamamura*

Department of Medicinal Chemistry, Institute of Biomaterials and Bioengineering, Tokyo Medical and Dental University, 2-3-10 Kandasurugadai, Chiyoda-ku, Tokyo 101-0062, Japan

Received August 18, 2010; E-mail: nomura.mr@tmd.ac.jp; tamamura.mr@tmd.ac.jp

Abstract: To date, challenges in the design of bivalent ligands for G protein-coupled receptors (GPCRs) have revealed difficulties stemming from lack of knowledge of the state of oligomerization of the GPCR. The synthetic bivalent ligands with rigid linkers that are presented here can predict the dimer form of CXCR4 and be applied to molecular probes in cancerous cells. This "molecular ruler" approach would be useful in elucidating the details of CXCR4 oligomer formation.

The chemokine receptor CXCR4 is a membrane protein belonging to the family of G protein-coupled receptors (GPCRs). In current drugs, ~60% of drug target molecules are located at the cell surface, and half of them are GPCRs.[1] Recent studies have indicated a pivotal role for homo- and heterooligomerization of CXCR4 in cancer metastasis, and the significance of oligomeric forms of GPCR has been gaining acceptance.[2] However, the functional implications proposed for these oligomers, which include signal transduction and internalization, are poorly understood and require additional studies.[3] Efforts to understand those correlations have used photochemical analyses such as bioluminescence resonance energy transfer (BRET) analysis,[3,4] but the elucidation of the native state of CXCR4 in living cells is complicated by conformational or functional changes resulting from mutations. Estimates of the precise distance between ligand binding sites in the dimer form would permit the development of bivalent ligands of CXCR4 having improved binding affinity and specificity.[5] In spite of the enormous effort devoted to the design of bivalent ligands, rational design of such linkers has been difficult because of the lack of knowledge concerning the dimeric form of GPCRs. Therefore, there is an increasing demand for a novel strategy for the analysis of the precise distance between ligand binding sites.[6]

In this study, we designed and synthesized novel CXCR4 bivalent ligands consisting of two molecules of an FC131[7] analogue, [*cyclo*(-D-Tyr-Arg-Arg-Nal-D-Cys-)] [Nal = L-3-(2-naphthyl)alanine, **1a**], connected by a poly(L-proline) or a PEGylated poly(L-proline) linker. Poly(L-prolines) have been utilized as rigid linkers between the two functional units, which require a predetermined separation for activity.[8] Linkers consisting of poly(L-prolines) were expected to maintain constant distances of 2−8 nm between the ligands. Our bivalent ligands with linkers of various lengths were used to determine the distance between two binding sites of ligands consisting of CXCR4 dimers. Acetamide-capped FC131 (**1b**), in which Gly is replaced by D-Cys and the thiol group of Cys is capped with an acetamide group, was synthesized as a monomer unit of the ligand (Figure 1). Although this substitution caused a 2-fold decrease in binding to CXCR4, the binding affinity was still adequate for analyses. Poly(L-proline) helices are known to maintain a length of 0.9 nm per turn.[9] In this study, polyproline- and

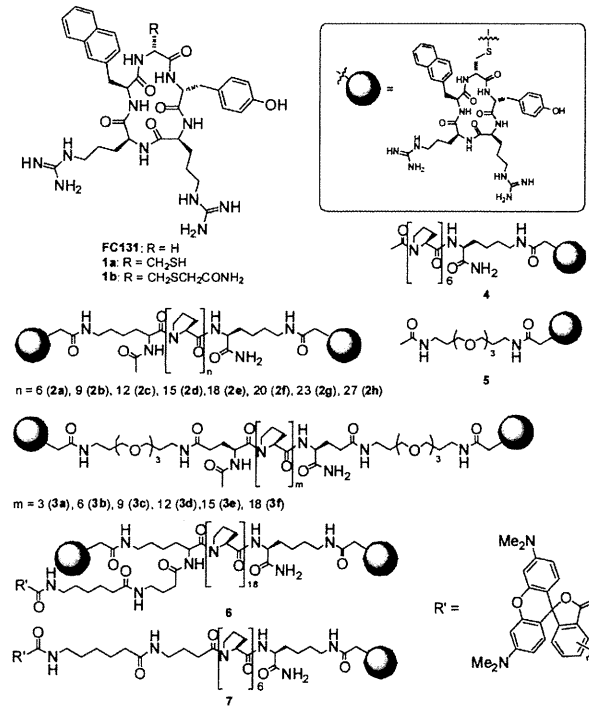

Figure 1. Design of bivalent ligands against chemokine receptor CXCR4. As CXCR4 binding moieties, D-Cys FC131 (R = CH_2SH, **1a**) and acetamide-capped FC131 (R = $CH_2SCH_2CONH_2$, **1b**) were prepared. Poly(L-proline) (**2a**−**h**) and PEG-conjugated poly(L-proline) (**3a**−**f**) with CXCR4 binding moieties on both ends were synthesized. As monomer binding ligands with linkers, Ac6pro FC131 (**4**) and AcPEG FC131 (**5**) were synthesized. Tetramethylrhodamine (TAMRA)-labeled **2e** (**6**) and **4** (**7**) were prepared for the imaging experiments.

PEGylated polyproline-type linkers with lengths of 2−8 nm were synthesized.[10] The synthetic linkers and their conjugated bivalent ligands were characterized by high-resolution mass spectrometry (HRMS) (Tables S3 and S5 in the Supporting Information), and their CD spectra clearly showed the presence of a type-II polyproline helix (Figure S3 in the Supporting Information). As monomer controls, FC131 analogues **4** and **5** with hexaproline and poly(ethylene glycol) (PEG) linkers, respectively, that were acetylated at the other end were also prepared.

The binding affinities of the synthetic ligands were evaluated in a competitive binding assay against [^{125}I]-SDF-1α, as reported previously.[7d] The binding assay showed that the binding affinity of our bivalent ligands is clearly dependent on the linker length. Ligands of the poly(L-proline) type with the highest affinities were **2e** and **2f**. Among the PEGylated poly(L-proline)-type ligands, **3c** and **3d** showed the highest affinity. The linker-optimized bivalent ligands, **2f** and **3d**, showed 7.3- and 21-fold increases in binding affinity relative to **4** and **5**, respectively (Table 1). These results

10.1021/ja107447w

Table 1. Summary of Binding Affinities of Synthetic Bivalent and Monovalent Ligands Analyzed by [^{125}I]-SDF-1α Competition Assay

compd	K_i (nM)[a]	linker length (nm)	compd	K_i (nM)[a]	linker length (nm)
FC131	31.5	–	**3a**	87.2	3.8
1b	53.4	–	**3b**	45.6	4.7
2a	51.2	1.8	**3c**	17.8	5.6
2b	45.4	2.7	**3d**	13.9	6.5
2c	64.4	3.6	**3e**	49.3	7.4
2d	59.5	4.5	**3f**	83.3	8.3
2e	13.2	5.4	**4**	72	–
2f	9.9	6	**5**	294	–
2g	22.5	6.9	**7**	119	–
2h	45.8	8.1			

[a] K_i values are the concentrations corresponding to 50% inhibition of [^{125}I]-SDF-1α binding to Jurkat cells.

indicate successful bivalent binding of the ligands, which has been known to be responsible for an increase in binding affinity.[5a] It should be noted that the maximum increase in binding affinity was observed for ligands of the two linker types having similar lengths (5.5–6.5 nm). In the dimer state of CXCR4, there are several forms of assembly (head-to-head, tail-to-tail, and head-to-tail).[5a] These forms have different distances between the binding sites of the ligands. Molecular modeling studies of FC131 with CXCR4 suggested that amino acids in transmembrane (TM) 7 are important for FC131 binding.[11] Through the use of the rhodopsin structure, it was revealed that in the TM 4 and 5 assembly form, the linear distance between ligand binding sites is 5.3 nm. In the other forms of possible assembly, the linear distances were determined to be 3.5 and 3.9 nm for TM 1 and 2 assembly and the combination of TM 1–4 and TM 2–5 assembly, respectively (Figure S4). The changes in binding affinity were relatively moderate, and although the existence of different assembly forms is possible, a majority of the population should be in the TM 4 and 5 assembly form.

From the increased binding affinity of linker-optimized bivalent ligands, a hypothesis was derived that such ligands could be applied as probes specific to CXCR4 on the cell surface because the receptors are overexpressed in several kinds of malignant cells[12] and that the dimer formation of the receptor should depend on the expression level. Accordingly, compound **2e**, which showed high binding affinity, was chosen for labeling with tetramethylrhodamine (TAMRA) and applied to the imaging of CXCR4. The TAMRA moiety was conjugated to an N-teminal of the proline linker via γ-butyric acid. To confirm that the ligands specifically bind to CXCR4, a CXCR4–EGFP fusion protein (EGFP = enhanced green fluorescent protein) was transiently expressed in HeLa cells. The increase in binding affinity of the bivalent ligand was clearly reflected in the imaging of CXCR4, as a merged image of TAMRA-labeled **2e** (**6**) and EGFP-fused CXCR4 was observed (Figure 2). When a control monomer, TAMRA-labeled **4** (**7**), was utilized for detection, only a trace of binding was observed. Additionally, binding to mock HeLa cells at the same concentration of ligands was not observed for either ligand (Figure S5).

To further evaluate the binding specificity and dependence on CXCR4 expression levels, fluorescence-activated cell sorting (FACS) analyses utilizing Jurkat, K562, and HeLa cells were performed (Figure 3). The cells were adopted on the basis of their different levels of CXCR4 expression (Jurkat > HeLa > K562).[13] The binding was evaluated by changes in mean fluorescence intensity (MFI) of the above cells in the presence and absence of ligands. The bivalent ligand **6** showed intense binding to Jurkat cells, which highly express CXCR4, as evidenced by the 2.3- and 3.3-fold increases in MFI at 25 and 250 nM, respectively. For binding to HeLa cells, the MFI was increased 2.4-fold by binding

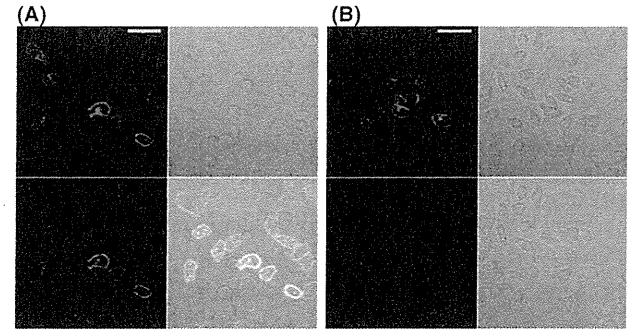

Figure 2. Binding of TAMRA-labeled FC131-derived monovalent and bivalent ligands to EGFP–CXCR4-transfected HeLa cells. Bivalent ligand **6** with an optimized linker length was utilized. The pictures show the binding of (A) **6** (25 nM) and (B) **7** (50 nM). Each panel is divided into four sections as follows: upper left, EGFP emission; upper right, differential interference contrast (DIC) image; lower left, TAMRA emission conjugated to ligands; lower right, merged image. Orange bars in the panels represent 50 μm.

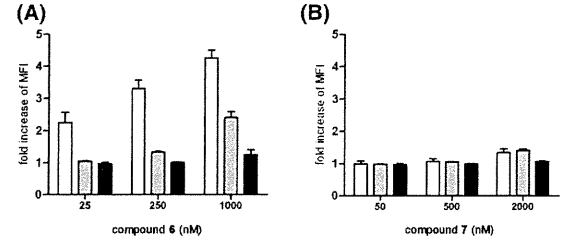

Figure 3. FACS analysis to evaluate the dependence of ligand binding on the levels of CXCR4 expression. The columns show the binding of (A) **6** and (B) **7** to Jurkat (white), HeLa (gray), and K562 (black) cells. The fold increase values were calculated by dividing the MFIs of the above cells in the presence of ligands by the corresponding values in the absence of ligands. The results are means of three independent experiments; error bars indicate standard errors of the mean.

of ligand **6** at 1 μM, although no significant increase in MFI was observed at 25 or 250 nM **6**, which corresponds with the imaging experiment (Figure S5). Meanwhile, the monovalent ligand **7** at 2 μM showed similar binding to Jurkat and HeLa cells, involving 1.1- and 1.4-fold increases in MFI, respectively. These results suggest that it is difficult to distinguish the expression level of CXCR4 by molecular imaging using the monovalent ligand. On the other hand, it is of special interest that the bivalent ligand showed distinguishability of the differences in CXCR4 expression levels. Furthermore, the binding of our CXCR4 ligands would be responsive to CXCR4, as no binding of either ligand to K562 cells, which express a trace of CXCR4, was observed. These results provide evidence in support of the hypothesis that the bivalent ligand binds preferentially to the constitutive dimer of CXCR4. Molecular imaging of CXCR4 on the cell surface by specific antibodies, such as c8352[14] or the monomer ligand T140,[15] has been previously reported. In the present system, however, it is possible that the bivalent ligands could distinguish the density of CXCR4 on the cell surface.

To further assess whether our bivalent ligand could distinguish between cancerous and normal cells by the imaging method, A549 and Human Umbilical Vein Endothelial Cells (HUVEC) were employed for staining as adhesive cell lines. A549 cells are human lung adenocarcinomic human alveolar basal epithelial cells, which are known to possess high CXCR4 expression levels.[16] HUVEC were chosen as a normal cell line without CXCR4 expression. It has been reported that the expression of CXCR4 on HUVEC is induced by fibroblast growth factor (FGF), which is highly expressed in the embryonic stage.[17] Thus, HUVEC was cultured

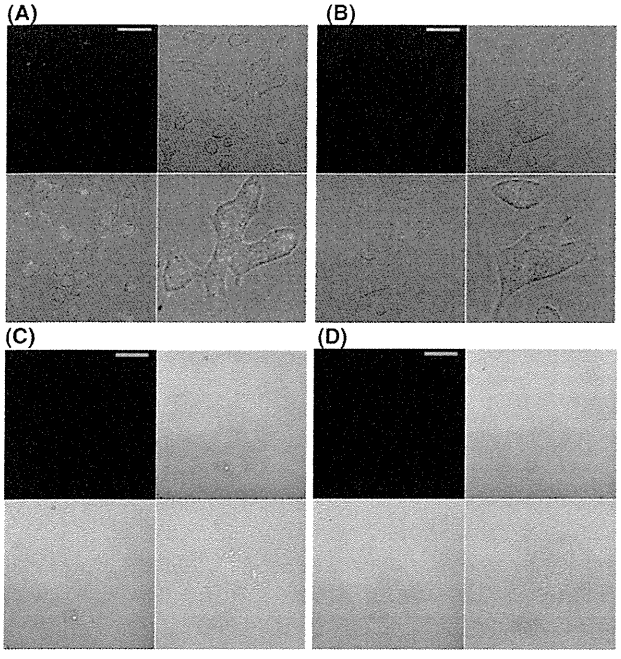

Figure 4. Imaging of CXCR4 by TAMRA-labeled FC131-derived monovalent and bivalent ligands on cancerous and normal primary cells. The panels show the binding of (A) **6** (1 μM) and (b) **7** (2 μM) to A549 cells and (C) **6** (250 nM) and (D) **7** (500 nM) to HUVEC cells. Each panel is divided into four sections as follows: upper left, TAMRA emission image; upper right; DIC image; lower left, merged image; lower right, focused image. Orange bars in the panels represent 50 μm.

in the absence of FGF. Ligand **6** showed clear binding to A549 cells (Figure 4A) but not to HUVEC (Figure 4C) at concentrations of 1 μM and 250 nM, respectively. On the other hand, monomer ligand **7** showed a trace of binding to each cell line (Figure 4B,D). Bivalent ligand **6** showed binding to HUVEC cultured with FGF at 250 nM (Figure S7). Thus, the bivalent ligands can detect cancerous cells that are in a state of high CXCR4 expression in a specific manner.

In summary, we have presented experimental results concerning the elucidation of the native state of the CXCR4 dimer utilizing bivalent ligands. These lead to a more precise understanding of the oligomerization state. Such a "molecular ruler" approach could be utilized in the design of bivalent ligands for any GPCR. It has been suggested that several GPCRs also exist as heterodimer forms, and CXCR4 has been hypothesized to form heterodimers with CCR2,[18] CCR5,[19] CXCR7,[4b] and the δ-opioid receptor.[20] Although the biological significance of GPCRs in homo- or heterooligomerization is still unclear and controversial, the approach described here involving rigid linkers conjugated to ligands specific to each GPCR would lead to elucidation of these issues. Furthermore, through the avidity shown as the specific binding affinity for the dimeric form of CXCR4, the fluorescent-labeled bivalent ligands have been shown to be powerful tools for cancer diagnosis on the basis of their ability to distinguish the density of CXCR4 on the cell surface. Our approach has the advantages that the ligand can directly capture dimeric forms of GPCRs and that the linkers can be applied to virtually any known GPCR.

Acknowledgment. The authors thank Prof. Kazunari Akiyoshi (Tokyo Medical and Dental University) for access to the laser scanning microscope. T.T. was supported by JSPS Research Fellowships for Young Scientists. This research was supported in part by New Energy and Industrial Technology Development Organization (NEDO).

Supporting Information Available: Curve-fitting data for the binding analyses, CD spectra, docking study of bivalent ligand binding, imaging analyses of mock cells, histogram and MFI of FACS analysis, imaging analyses of HeLa cells cultured with FGF, experimental procedures, and spectral and analytical data for all new compounds. This material is available free of charge via the Internet at http://pubs.acs.org.

References

(1) Overington, J. P.; Al-Lazikani, B.; Hopkins, A. L. *Nat. Rev. Drug. Discovery* **2006**, *5*, 993–996.
(2) Wang, J.; He, L.; Combs, C. A.; Roderiquez, G.; Norcross, M. A. *Mol. Cancer Ther.* **2006**, *5*, 2474–2483.
(3) Percherancier, Y.; Berchiche, Y. A.; Slight, I.; Volkmer-Engert, R.; Tamamura, H.; Fujii, N.; Bouvier, M.; Heveker, N. *J. Biol. Chem.* **2005**, *280*, 9895–9903.
(4) (a) Babcock, G. J.; Farzan, M.; Sodroski, J. *J. Biol. Chem.* **2003**, *278*, 3378–3385. (b) Luker, K. E.; Gupta, M.; Luker, G. D. *FASEB J.* **2009**, *23*, 823–834.
(5) (a) Handl, H. L.; Sankaranarayanan, R.; Josan, J. S.; Vagner, J.; Mash, E. A.; Gillies, R. J.; Hruby, V. J. *Bioconjugate Chem.* **2007**, *18*, 1101–1109. (b) Zheng, Y.; Akgün, E.; Harikumar, K. G.; Hopson, J.; Powers, M. D.; Lunzer, M. M.; Miller, L. J.; Portoghese, P. S. *J. Med. Chem.* **2009**, *52*, 247–258.
(6) Panetta, R.; Greenwood, M. T. *Drug Discovery Today* **2008**, *13*, 1059–1066.
(7) (a) Tamamura, H.; Xu, Y.; Hattori, T.; Zhang, X.; Arakaki, R.; Kanbara, K.; Omagari, A.; Otaka, A.; Ibuka, T.; Yamamoto, N.; Nakashima, H.; Fujii, N. *Biochem. Biophys. Res. Commun.* **1998**, *253*, 877–882. (b) Fujii, N.; Oishi, S.; Hiramatsu, K.; Araki, T.; Ueda, S.; Tamamura, H.; Otaka, A.; Kusano, S.; Terakubo, S.; Nakashima, H.; Broach, J. A.; Trent, J. O.; Wang, Z.; Peiper, S. C. *Angew. Chem., Int. Ed.* **2003**, *42*, 3251–3253. (c) Tamamura, H.; Araki, T.; Ueda, S.; Wang, Z.; Oishi, S.; Esaka, A.; Trent, J. O.; Nakashima, H.; Yamamoto, N.; Peiper, S. C.; Otaka, A.; Fujii, N. *J. Med. Chem.* **2005**, *48*, 3280–3289. (d) Tanaka, T.; Tsutsumi, H.; Nomura, W.; Tanabe, Y.; Ohashi, N.; Esaka, A.; Ochiai, C.; Sato, J.; Itotani, K.; Murakami, T.; Ohba, K.; Yamamoto, N.; Fujii, N.; Tamamura, H. *Org. Biomol. Chem.* **2008**, *6*, 4374–4377.
(8) (a) Arora, P. S.; Ansari, A. Z.; Best, T. P.; Ptashne, M.; Dervan, P. B. *J. Am. Chem. Soc.* **2002**, *124*, 13067–13071. (b) Sato, S.; Kwon, Y.; Kamisuki, S.; Srivastava, N.; Mao, Q.; Kawazoe, Y.; Uesugi, M. *J. Am. Chem. Soc.* **2007**, *129*, 873–880.
(9) (a) Kuemin, M.; Schweizer, S.; Ochsenfeld, C.; Wennemers, H. *J. Am. Chem. Soc.* **2009**, *131*, 15474–15482. (b) Schuler, B.; Lipman, E. A.; Steinbach, P. J.; Kumke, M.; Eaton, W. A. *Proc. Natl. Acad. Sci. U.S.A.* **2005**, *102*, 2754–2759.
(10) For synthesis details, see the Supporting Information.
(11) Våbenø, J.; Nikiforovich, G. V.; Marshall, G. R. *Chem. Biol. Drug Des.* **2006**, *67*, 346–354.
(12) Balkwill, F. *Semin. Cancer Biol.* **2004**, *14*, 171–178.
(13) (a) Carnec, X.; Quan, L.; Olson, W. C.; Hazan, U.; Dragic, T. *J. Virol.* **2005**, *79*, 1930–1933. (b) Majka, M.; Rozmyslowicz, T.; Honczarenko, M.; Ratajczak, J.; Wasik, M. A.; Gaulton, G. N.; Ratajczak, M. Z. *Leukemia* **2000**, *14*, 1821–1832.
(14) Schwartz, V.; Lue, H.; Kraemer, S.; Korbiel, J.; Krohn, R.; Ohl, K.; Bucala, R.; Weber, C.; Bernhagen, J. *FEBS Lett.* **2009**, *583*, 2749–2757.
(15) Nomura, W.; Tanabe, Y.; Tsutsumi, H.; Tanaka, T.; Ohba, K.; Yamamoto, N.; Tamamura, H. *Bioconjugate Chem.* **2008**, *19*, 1917–1920.
(16) Murdoch, C.; Monk, P. N.; Finn, A. *Immunology* **1999**, *98*, 36–41.
(17) Salcedo, R.; Wasserman, K.; Young, H. A.; Grimm, M. C.; Howard, O. M. Z.; Anver, M. R.; Kleinman, H. K.; Murphy, W. J.; Oppenheim, J. J. *Am. J. Pathol.* **1999**, *154*, 1125–1135.
(18) Sohy, D.; Parmentier, M.; Springael, J. *J. Biol. Chem.* **2007**, *282*, 30062–30069.
(19) Contento, R. L.; Molon, B.; Boularan, C.; Pozzan, T.; Manes, S.; Marullo, S.; Viola, A. *Proc. Natl. Acad. Sci. U.S.A.* **2008**, *105*, 10101–10106.
(20) Pello, O. M.; Martínez-Muñoz, L.; Parrillas, V.; Serrano, A.; Rodríguez-Frade, J. M.; Toro, M. J.; Lucas, P.; Monterrubiol, M.; Martínez-A, C.; Mellado, M. *Eur. J. Immunol.* **2008**, *38*, 537–549.

JA107447W

Development of Crosslink-Type Tag-Probe Pairs for Fluorescent Imaging of Proteins

Wataru Nomura, Tomoaki Mino, Tetsuo Narumi, Nami Ohashi, Akemi Masuda, Chie Hashimoto, Hiroshi Tsutsumi, Hirokazu Tamamura

Institute of Biomaterials and Bioengineering, Tokyo Medical and Dental University, Chiyoda-ku, Tokyo 101-0062, Japan

Received 29 January 2010; revised 15 March 2010; accepted 23 March 2010
Published online 4 August 2010 in Wiley Online Library (wileyonlinelibrary.com). DOI 10.1002/bip.21444

ABSTRACT:

Useful methods of protein labeling via functional peptide tags have been developed in the field of proteome and chemical biology. New tag-probe pairs based on leucine zipper peptides for labeling target proteins are described. These consist of an α-helical probe peptide with an environmental-sensitive fluorescent dye and two antiparallel α-helical tag peptides, and may be crosslinked, from the Cys residue of the tag peptide to the N^{α}-chloroacetyl group of the probe peptide. Binding of the probe peptide to the tag peptides results in movement of the fluorophore from a hydrophilic to a hydrophobic environment inside the leucine zipper structure, causing a dramatic fluorescent change, mediated by the binding of the two peptides. As a spacer between the N^{α}-chloroacetyl group and the original probe sequence, a single Gly residue was the most suitable among 0-2 Gly residues. Crosslinking leads to superior fluorescence response, binding affinity, and chemical stability. These ZIP tag-probe pairs are useful for labeling and fluorescent imaging of proteins. © *2010 Wiley Periodicals, Inc. Biopolymers (Pept Sci) 94: 843-852, 2010.*

Keywords: crosslinking; environmental-sensitive fluorescent dye; fluorogenic tag-probe pair; leucine zipper; protein imaging

Correspondence to: Hirokazu Tamamura; e-mail: tamamura.mr@tmd.ac.jp
Contract grant sponsors: Ministry of Education, Culture, Sports, Science and Technology, Japan, the Japan Health Science Foundation

This article was originally published online as an accepted preprint. The "Published Online" date corresponds to the preprint version. You can request a copy of the preprint by emailing the Biopolymers editorial office at biopolymers@wiley.com

INTRODUCTION

In the post-genome era, artificial peptide tools have been used in the field of proteome and chemical biology. In the fluorescent imaging of proteins in living systems, several pairs of peptide tags and their complementary probes have been found to be useful tools. Short peptides which include an oligohistidine tag (His tag) can be incorporated into target proteins and then applied to the purification of recombinant proteins and immobilization of proteins on plates with their complementary molecules, such as the Ni(II)-nitrilotriacetic acid complex (Ni(II)-NTA).[1,2] A His tag has been utilized for fluorescent imaging of proteins in cells using Ni(II)-NTA derivatives with an appended fluorophore.[3–5] In addition, pairs of tetracysteine motif peptides and biarsenical molecular probes, which specifically bind to a tetracysteine sequence, are useful in the real-time fluorescent imaging of cellular proteins.[6,7] Other pairs of short tag peptides and their specific ligands have also been reported.[8–11] A variety of engineered protein tags such as the SNAP tag and the Halo tag have been also reported to be useful in the fluorescent imaging of proteins,[12–15] but in these cases a washing step to remove excess probe molecules, which do not bind to the tag, is required to avoid their background emission. The binding of probes to target proteins via their complementary tags is accompanied by a drastic shift of fluorescent wavelength and/or an increase of fluorescence intensity, facilitating distinction of the labeled proteins and the free probes. Thus, further development of such novel fluorogenic tag-probe pairs is useful and desirable.

Leucine zipper peptides involving three α-helical antiparallel strands have been utilized as tags for the affinity purifi-

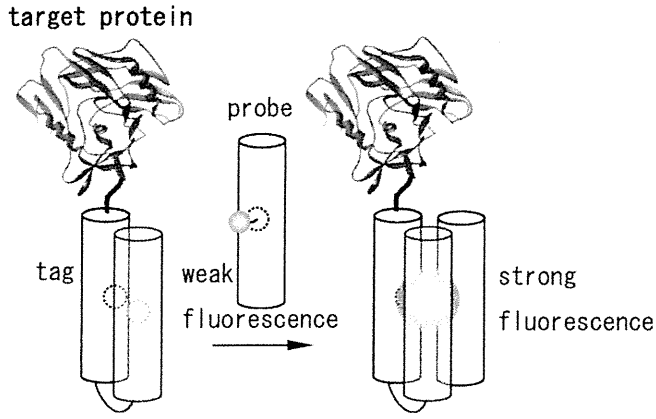

FIGURE 1 Formation of tag-probe pairs with fluorogenic activity based on the artificial leucine zipper peptides, designated as ZIP tag-probe pairs, and their application to the fluorescent imaging of ZIP tag-fused proteins.

cation of recombinant proteins[16] and as anchors for the immobilization of proteins on micro plates.[17] Complementary selectivity and strong binding affinity have prompted application of new tag-probe pairs to the bio-imaging of proteins. Since hydrophobic cores of leucine zipper peptides can be adjusted to form hydrophobic pockets in which small molecules can bind,[18,19] selective binding of environmentally sensitive fluorescent dyes to these pockets inside the leucine zipper assembly might lead to colorimetric changes and enhance their fluorescence intensity. Accordingly, we have developed new tag-probe pairs with fluorogenic activity based on the artificial leucine zipper peptides, designated as ZIP tag-probe pairs, and applied them to the fluorescent imaging of ZIP tag-fused protein on the surface of living cells (see Figure 1).[20]

The design of ZIP tag-probe pairs was based on the crystal structure of an antiparallel coiled-coil trimer of a GCN4 mutant shown in Figure 2.[21] A probe peptide consists of an α-helical peptide in which 4-nitrobenzo-2-oxa-1,3-diazole (NBD), an environmentally sensitive fluorescent dye is imbedded. The NBD is attached to the side chain of the L-α-2,3-diaminopropionic acid residue (Dap(NBD)) at position 13 on the hydrophobic site of the leucine zipper structure. A tag peptide consists of antiparallel 2 α-helical peptides linked via a Gly-Gly-Cys-Gly-Gly loop sequence. Two Leu residues in the tag peptide, located at the positions complementary to the Dap(NBD) residue of the probe peptide, are replaced by Ala so that an adequate hydrophobic pocket is formed when the tag peptide binds to the probe peptide.

In fluorescent titration analysis, the change in the fluorescence spectra of the probe peptide depends largely on the concentration of the tag peptide. The emission spectra derived from NBD showed a 17-fold increase in emission intensity with a concomitant blue shift of the emission maximum from 535 nm to 505 nm (see Figure 3). This spectral change shows that the NBD moiety of the probe peptide is located in the hydrophobic environment inside the 3α-helical peptide bundle structure. The dissociation constant of the probe peptide toward the tag peptide, was estimated by analysis of the fluorescent titration curve with a nonlinear least-squares curve fitting method[22] at 18 n*M*. The tag-probe pair was also applied to the fluorescent imaging of the tag-fused CXCR4 by the probe peptide in the living cells. CXCR4 is a member of a chemokine receptor family, involving seven transmembrane G-protein coupled receptor (7TM-GPCR) families.[23,24] The tag-fused CXCR4, in which the tag is genetically fused to the extracellular N-terminus region of CXCR4, is transiently expressed on the surface of CHO-K1 cells. Sequential labeling experiments of the tag-fused CXCR4 using the probe peptide with the NBD dye and a fluorescent CXCR4 antagonist were performed. In the presence of the excess probe peptide, the labeling of tag-fused CXCR4 using the probe peptide with NBD produced bright green fluorescence on the surface of the cells (see Figure 4).[25] Subsequently, the tag-fused CXCR4 was stained in a red color by the CXCR4 antagonist, tetramethylrhodamine (TAMRA)-appended T140. In this way, a membrane protein CXCR4 can be successfully visualized using the ZIP tag-probe system which this is shown to be a useful fluorescent imaging tool for proteins in living cells. The tag-probe complex consist-

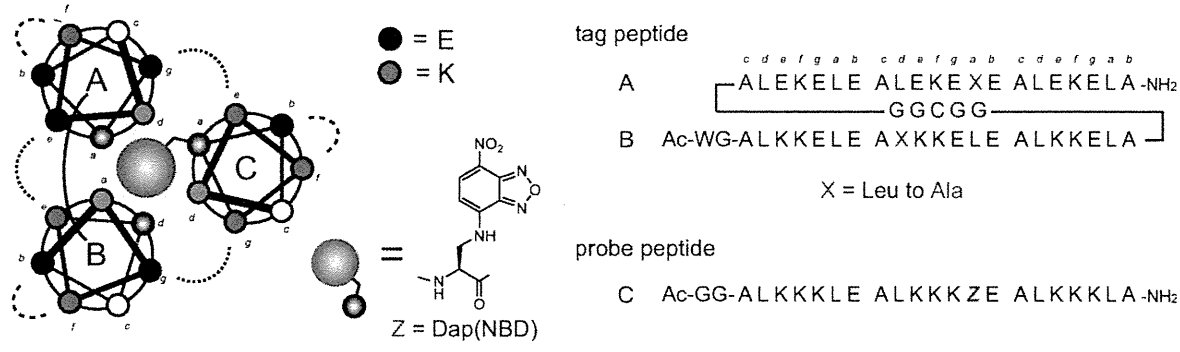

FIGURE 2 Design and structure of ZIP tag-probe pairs.

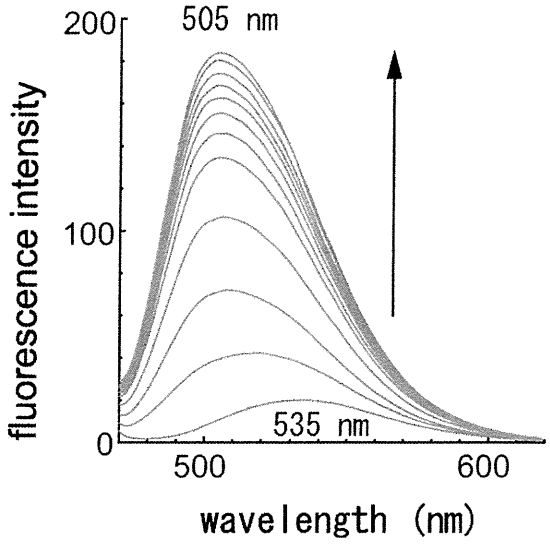

FIGURE 3 Fluorescence spectral change of the probe peptide upon the addition of the tag peptide at 25°C in 50 m*M* HEPES buffer (pH 7.2, 100 m*M* NaCl): [probe] = 0.5 μM, [tag] = 0 to 2.0 μM.

ing of the antiparallel 3α-helical peptide bundle structure is formed as a result of the affinity of the tag peptide and the probe peptide. Since this interaction involves noncovalent bonds, introduction of crosslink by a covalent bond might increase chemical and biological stability. Thus, we developed tag-probe pairs, crosslinked by covalent bonds (see Figure 5).

RESULTS AND DISCUSSTION

Crosslinking Reaction of the Tag Peptide With the Probe Peptide

To investigate the optimum length of crosslinkers, three types of probe peptides with linkers of different lengths were synthesized. The original tag peptide has a side-chain thiol group in the Gly-Gly-Cys-Gly-Gly loop structure between antiparallel 2α-helical peptides. At the N-terminus of each probe peptide, 0, 1, or 2 Gly residues were attached as a spacer and an N^{α}-chloroacetyl group as a functional group for coupling with the Cys thiol group (see Figure 6). The probe peptides having 0, 1, and 2 Gly residues were designated probe **1**, **2**, and **3**. As control probe peptides, probe peptide **4**, which has no chloroacetyl group, and **5**, which has N^{ε}-chloroacetyl-Lys at the C-terminus, both possessing N^{α}-acetyl-Gly, were also prepared. Probe peptides **1**-**5** were prepared by Fmoc-based solid-phase peptide synthesis.[26] The tag peptide was prepared by native chemical ligation[27,28] of the synthetic C-terminal thioester fragment A and the N-terminal cysteine fragment B, which were divided at the cysteine residue of the loop sequence.[20] Using the probe peptides **1**-**3**, the crosslinking reactions with the tag peptide, monitored by HPLC,[29] were performed by addition of the tag peptide to the probe peptide (1:1, final 1 μM each) in 50 m*M* HEPES buffer, pH 7.2 containing 100 m*M* NaCl at room temperature. The time course of the crosslinking reaction of the probe peptide **2** is shown in Figures 7 and 8a. Peak areas of the tag peptide and the probe peptide **2** with the retention times of ~18 min and 32 min, respectively, decreased in a time-dependent manner, while that of the product of crosslink, the tag-probe **2** complex, with retention time of 28 min, increased. Completion of this reaction was the fastest of the crosslinking reactions, requiring approximately 20 min (Figure 8b). The order of the reaction rate of the probe peptides was **2**, **1**, **3**, and **5** (Figures 8b and 9). Reactions of **1** and **3** were mostly complete in 30 min, and the crosslinking reaction of the tag peptide with the probe peptide **5** failed (see Figure 9). These results suggest that a Gly residue at position 1 is the most suitable spacer and that the chloroacetyl group of the probe peptide and the thiol group of the tag peptide react in a structure-specific manner. In the use of the probe peptides **1**-**3** to form the tag-probe pairs, the chloroacetyl and thiol groups approach one another prior to the cross-

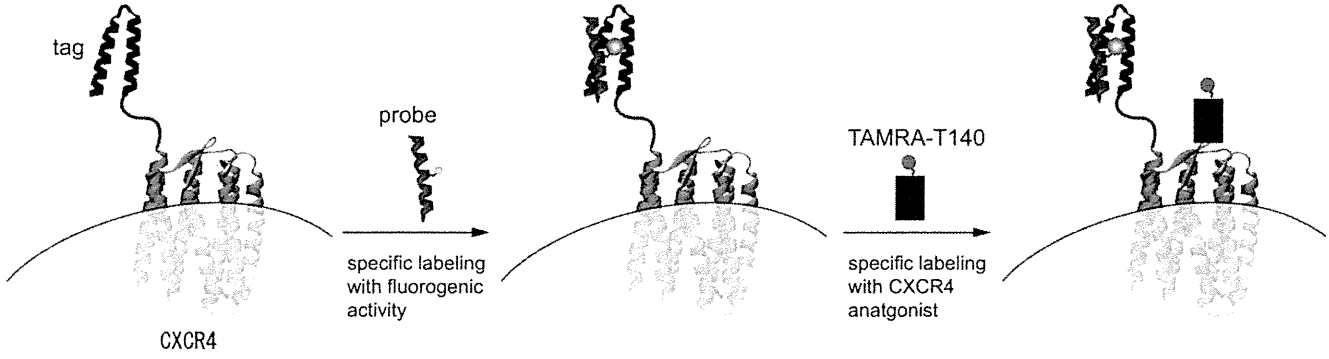

FIGURE 4 Sequential labeling of the tag-fused CXCR4 on the cell surface by the TAMRA-appended CXCR4 antagonist T140 after the labeling by the probe peptide.

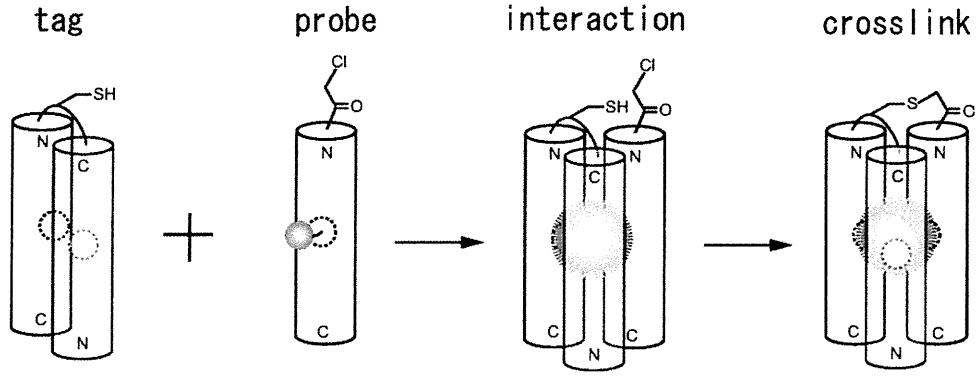

FIGURE 5 Crosslink-type ZIP tag-probe pairs with fluorogenic activity: formation of tag-probe pairs and the subsequent crosslink by a covalent bond.

linking reaction. In the case of the probe peptide **5**, when the tag-probe pair is formed the chloroacetyl and thiol groups are located quite separately on opposite sides and can not interact. All of the crosslink products were purified by RP-HPLC and characterized by ESI-MS.

Fluorescent Titration Analysis

In the fluorescent titration analysis of the addition of the tag peptide to the probe peptide **2**, the fluorescence spectra of **2** changed remarkably, depending on the concentration of the tag peptide. The emission maximum due to the NBD dye showed a significant blue shift from 537 nm to 504 nm with a 22-fold increase in the emission intensity (see Figure 10). Such a spectral change clearly suggests that the NBD moiety of the probe peptide is located in the hydrophobic environment inside the 3α-helical peptide bundle structure, as in noncovalent type formation of the ZIP tag-probe pair.[20] Comparison with the other probe peptides in the fluorescent titration analysis is shown in Figure 10b and Table I. In the use of all of the probe peptides, a similar blue shift of the emission maximum due to the NBD dye from 534–537 nm to 504 nm was observed. The increase of emission intensity, most remarkable in the case of probe peptide **2**, was in the order **2**, **1**, **3**, **4**, and **5**. This suggests that tag-probe **2** pair is most suitable for analytical purposes.

The dissociation constants of the probe peptides **1**, **2**, **3**, **4**, and **5** toward the tag peptide were estimated by analysis using nonlinear least-squares curve fitting[22] as 6.2 n*M*, 6.5 n*M*, 9.0 n*M*, 22 n*M*, and 12 n*M*, respectively (Table I). Thus, in terms of dissociation constant, the probe peptide **1** is comparable to **2**, indicating similar binding affinities, but the hydrophobic environment formed by the interaction of the tag peptide with the probe peptide **2** would appear to be more suitable for the fluorescence emission of the NBD dye.

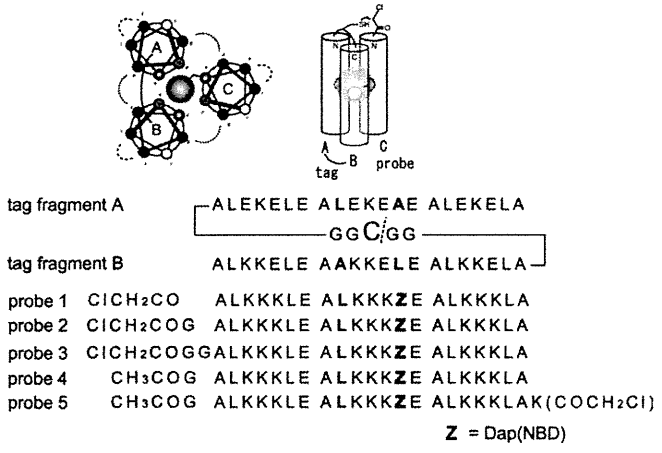

FIGURE 6 Design and structure of crosslink-type ZIP tag-probe pairs. Probe peptides **1**-**3** have an N^{α}-chloroacetyl group at the N-terminus. Probe peptides **4** and **5** have an N^{α}-acetyl group at the N-terminus. Probe peptide **5** has N^{ε}-chloroacetyl-Lys at the C-terminus.

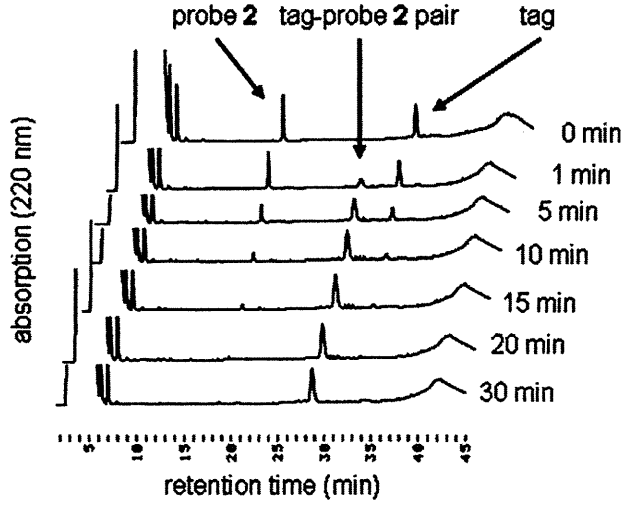

FIGURE 7 HPLC monitoring of the crosslinking reaction of the tag peptide with the probe peptide **2**. The reaction was performed by addition of the tag peptide to the probe peptide **2** (1:1, final 1 μM each) in 50 m*M* HEPES buffer, pH 7.2 containing 100 m*M* NaCl at room temperature.

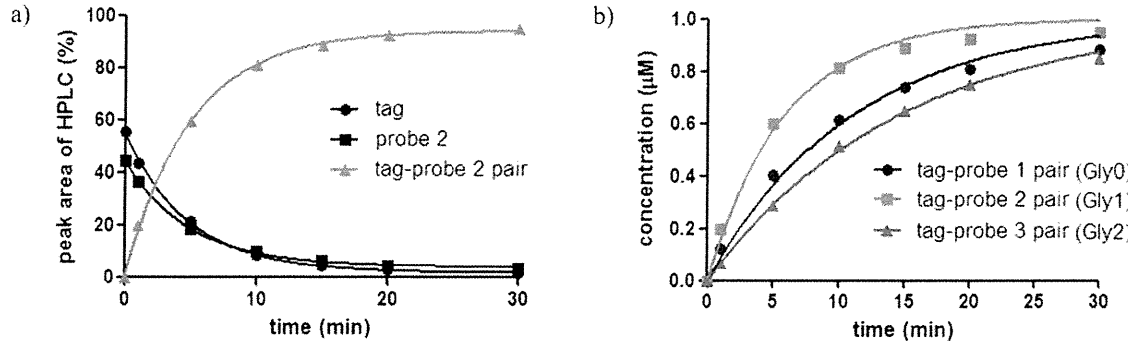

FIGURE 8 The time course of the crosslinking reaction of the tag peptide with the probe peptides. (a) The time course of HPLC peak areas of tag, probe **2** and tag-probe **2** pair, (b) the time course of concentrations of resulting tag-probe **1-3** pairs.

Compared with the noncovalent tag-probe **4** pair, whose dissociation constant is 22 n*M*, the affinities of the covalent type tag-probe **1**, **2**, and **3** pairs are remarkably higher, suggesting that crosslink of tag and probe peptides underlies the increase in affinity. In the tag-probe **5** pair, a similar spectral change was observed, indicating that the NBD dye was located in the hydrophobic pocket, although a covalent bond for crosslink of tag and probe peptides was apparently absent (see Figure 11).

Fluorescence Job's Titration

Fluorescent Job's titration, recording the intensity at 505 nm, was performed to assess the stoichiometry of the tag-probe **2** complex (see Figure 12). The total concentration of the probe peptide **2** and the tag peptide was fixed at 1.0 μM. The concentrations of the tag peptide were 0, 0.2, 0.4, 0.5, 0.6, 0.8, and 1.0 μM. This fluorescence Job's titration experiment clearly indicates that the probe peptide **2** binds to the tag peptide with 1:1 stoichiometry. The result suggests that the tag peptide and the probe peptides **1-3** form a stable 3α-helical leucine zipper structure by binding with 1:1 stoichiometry.

Investigation of Chemical Stability by Fluorescence Analysis

The chemical stability to thermal denaturation of the tag-probe complexes was investigated. Using the complexes of the tag peptide and the probe peptides **1-5**, changes of fluorescence intensity were monitored. The aqueous solution of 1 μM tag-probe complex in 50 m*M* HEPES buffer, pH 7.2 containing 100 m*M* NaCl was prepared, and then the temperature of the solution was gradually increased to 100°C. Fluorescence spectral changes of the tag-probe peptide **2** and **4** pairs, representatives of crosslink pairs and noncrosslink pairs, are shown in Figure 13. In Figure 14 changes of fluorescence intensity of the tag-probe peptide **1-5** pairs are shown. In each of the complexes of the tag peptide with probe peptides **1-5**, a gradual

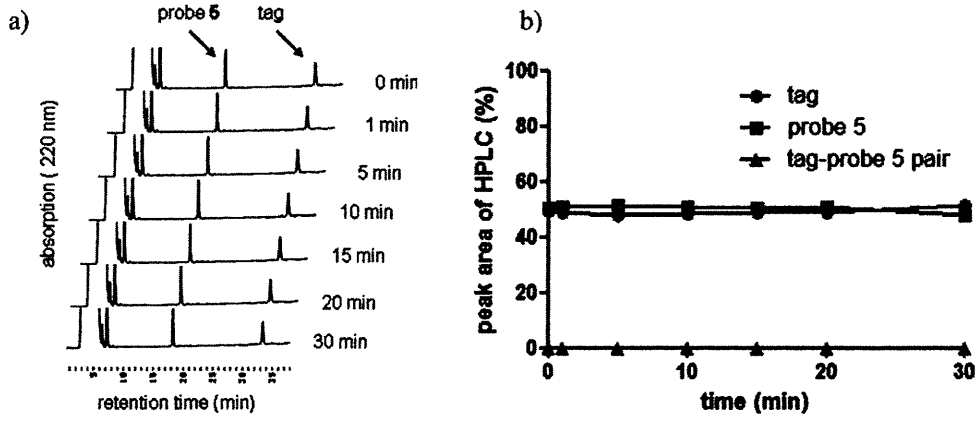

FIGURE 9 (a) HPLC monitoring of the crosslinking reaction of the tag peptide with the probe peptide **5**. The reaction was performed by addition of 1 μM tag peptide to 1 μM probe peptide **5** in 50 m*M* HEPES buffer, pH 7.2 containing 100 m*M* NaCl at room temperature. (b) The time course of HPLC peak areas of tag, probe **5** and tag-probe **5** pair.

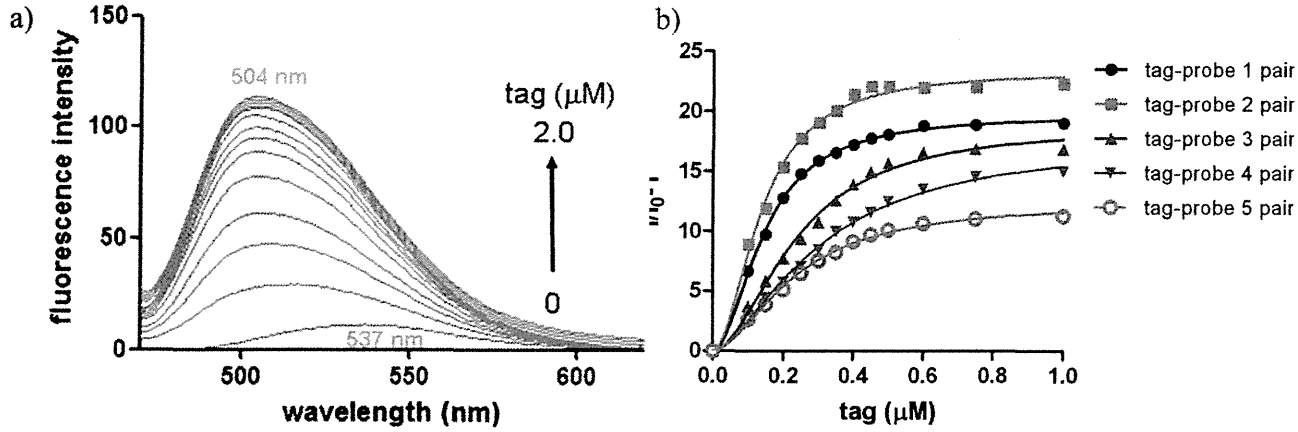

FIGURE 10 (a) Fluorescence spectral change of the probe peptide **2** upon the addition of the tag peptide at 25°C in 50 m*M* HEPES buffer (pH 7.2, 100 m*M* NaCl): [probe] = 0.5 μ*M*, [tag] = 0 to 2.0 μ*M*. (b) Change of fluorescence intensity of the probe peptides **1**-**5** upon the addition of the tag peptide for calculation of dissociation constants of tag-probe pairs.

decrease in fluorescence intensity was observed in proportion to the increase of temperature. The complexes of the tag peptide and the probe peptides **1**-**3** were more stable than those of **4** and **5**, which were completely denatured at 100°C, but the complexes using **1**-**3** were not denatured, possibly due to the crosslinking. The melting temperatures of the complexes using **1**-**3** were above 69°C, whereas those of the complexes involving **4** and **5** were below 56°C.

The possibility that this thermal denaturation is reversible was next investigated. The pairs of tag-probe **2** and tag-probe **4** were adopted as representative of crosslink pairs and non-crosslink pairs, respectively. After denaturing the tag-probe **2** pair at 100°C, the temperature of the solution was gradually decreased (Figure 15a). In proportion to the decrease of temperature, a gradual increase in fluorescence intensity of probe **2** was observed, resulting finally in complete recovery of the original fluorescence intensity. In contrast, while a gradual increase in fluorescence intensity, proportionate to a decrease in temperature, was also observed after the thermal denaturation at 100°C of tag-probe pair **4**, the fluorescence intensity recovered only to approximately half of its original level (Figure 15b). These results suggest that the crosslinking of tag and probe peptides is critical for complete reversibility of the fluorescence emission.

Table I Results of Fluorescence Titration of Tag-Probe Pairs

	Fluorescence Wavelength of Emission Maximum (nm)	I_{max}/I_0 (Fold)	Dissociation Constant (n*M*)[a]
Tag-probe **1** pair	537–504	19	6.2
Tag-probe **2** pair	537–504	23	6.5
Tag-probe **3** pair	535–504	17	9.0
Tag-probe **4** pair	534–504	15	22
Tag-probe **5** pair	534–504	11	12

[a] Measurement conditions: 50 m*M* HEPES buffer solution (pH 7.2, 100 m*M* NaCl), at 25°C, [probe] = 0.5 μ*M*.

Investigation of Chemical Stability by Circular Dichroism

The chemical stability of the tag-probe complexes to thermal denaturation was investigated by circular dichroism (CD). The CD spectra showed that all of the tag-probe **1**-**4** complexes form α-helical structures. The CD spectrum of the tag-probe **2** complex had the strongest double minima at 207 and 222 nm, while the spectrum of the non-covalent type tag-probe **4** complex showed the weakest double minima among the four complexes (see Figure 16). This result sug-

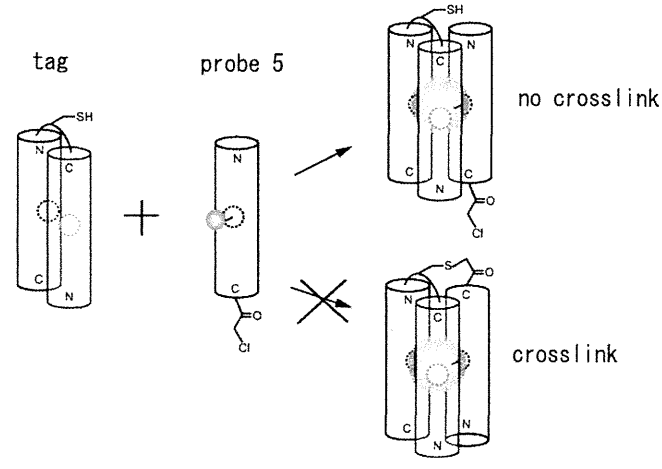

FIGURE 11 Formation of tag-probe **5** pair without crosslinking. When tag-probe **5** pair is formed, the chloroacetyl and thiol groups are separated, located on opposite sides and no covalent bond can form between them.

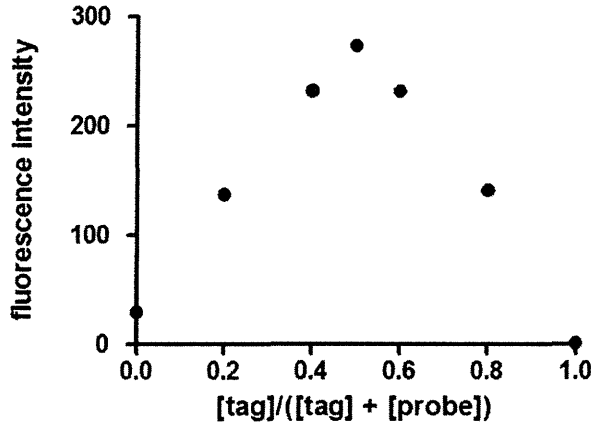

FIGURE 12 Fluorescence Job's titration between the probe peptide **2** and the tag peptide, [probe **2**] + [tag] = 1.0 μM, in 50 mM HEPES buffer (pH 7.2, 100 mM NaCl) at 25°C.

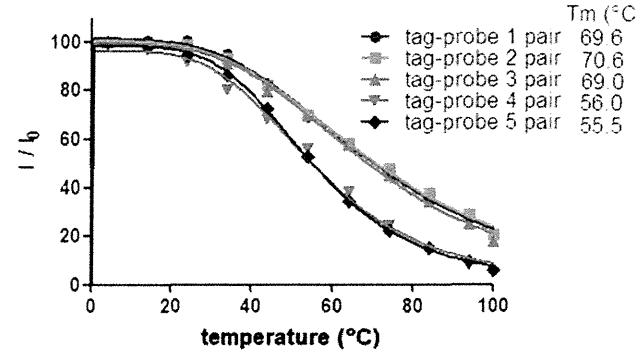

FIGURE 14 Change of fluorescence intensity of tag-probe **1-5** pairs from 4°C to 100°C in 50 mM HEPES buffer (pH 7.2, 100 mM NaCl): [tag-probe pair] = 0.5 μM. Values of melting temperature (T_m) of tag-probe peptide **1-5** pairs are shown.

gests that crosslinking of the tag and probe peptides is essential for the α-helical structures. Changes in [θ] at 222 nm in aqueous solution of 1 μM tag-probe pair in 50 mM Tris-HCl buffer, pH 7.2 containing 100 mM NaCl were monitored, and the temperature of the solution was gradually increased to 94°C (Figure 17a). In all the tag-probe **1-4** pairs, a gradual increase in values of [θ] at 222 nm was observed in proportion to the increase in temperature. Tag-probe **4** pair, in particular, showed a remarkable increase in values of [θ] at 222 nm, suggesting that the α-helical structures were largely collapsed. Judging by the changes of [θ] at 222 nm, the α-helical structures of tag-probe **1-3** pairs survived better than those of tag-probe **4** pair, possibly due to the crosslinking. Next, whether the above α-helical structures can be reversibly recovered was investigated (Figure 17b). The pairs of the tag peptide and the probe peptides **2** and **4** were adopted as representatives of crosslink pairs and noncrosslink pairs, respectively. After denaturing the tag-probe **2** and **4** pairs at 94°C, the temperature of the solution was gradually decreased., Gradual decreases in values of [θ] at 222 nm in proportion to the decrease of temperature were observed with both pairs. In the case of the tag-probe **2** pair the value of [θ] at 222 nm was finally nearly completely recovered but with the tag-probe **4** pair [θ] was not reduced to its original value, suggesting that the crosslink of tag and probe peptides is indispensable for complete reversibility of the α-helical structures.

CONCLUSION

The novel tag-probe pairs based on leucine zipper peptides, in which the thiol group of the Cys residue of the tag peptide and the chloroacetyl group of the probe peptide were crosslinked, have been studied. They were found to have significant fluorogenic activity, mediated by the binding of the tag peptide to the probe peptide as the noncrosslink-type pairs. Compared with noncrosslinked tag-probe pairs, those that are crosslinked were shown to have some advantages in terms of fluorescence

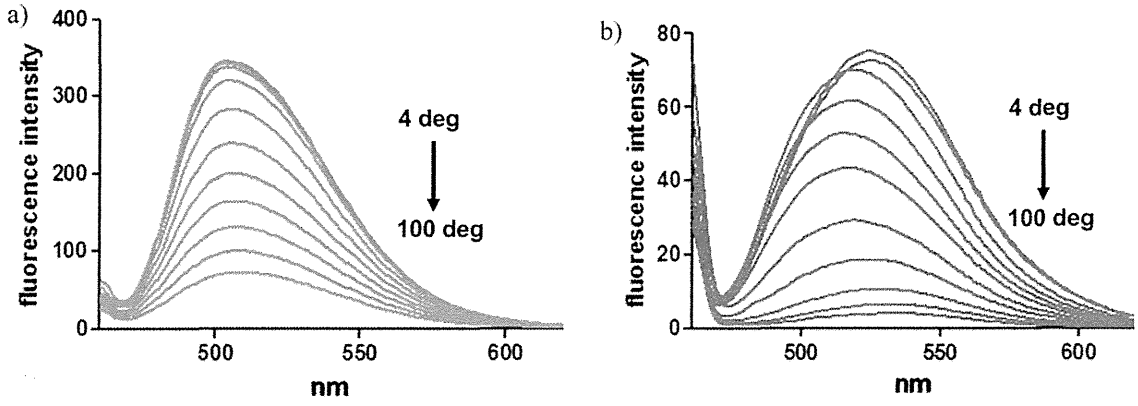

FIGURE 13 Fluorescence spectral change of tag-probe pairs from 4°C to 100°C in 50 mM HEPES buffer (pH7.2, 100 mM NaCl): [tag-probe pair] = 0.5 μM. (a) tag-probe **2** pair, (b) tag-probe **4** pair.

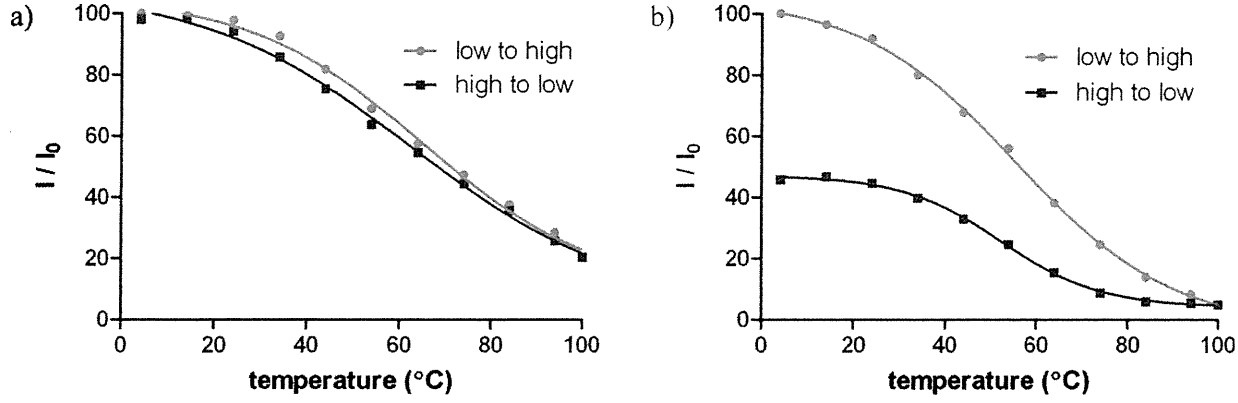

FIGURE 15 Change of fluorescence intensity of tag-probe pairs from 4°C to 100°C (low to high) and from 100°C to 4°C (high to low) in 50 m*M* HEPES buffer (pH 7.2, 100 m*M* NaCl): [tag-probe pair] = 0.5 μM. (a) tag-probe **2** pair, (b) tag-probe **4** pair.

response, binding affinity, and chemical stability. As a spacer between the N^{α}-chloroacetyl group and the original probe sequence, a single Gly residue was superior to 0 or 2 Gly residues. Thus, the probe peptide **2**, having the 1 Gly spacer, binds more rapidly to the tag peptide than the probe peptides **1** and **3**, with 0 and 2 Gly spacers, respectively. Both the previous noncrosslink-type and the present crosslink-type ZIP tag-probe pairs might facilitate the real-time imaging of target proteins without removal of excess probe molecules. Thus, the crosslink-type ZIP tag-probe pairs should be highly useful and valuable for studies of imaging of proteins in living cells.

EXPERIMENTAL PROCEDURES

General

HPLC was carried out on a reversed phase column with a LaChrom Elite HTA system (Hitachi). Matrix-assisted laser desorption/ionization time-of-flight mass spectrometry (MALDI-TOF-MS) was recorded on a Voyager DE-STR (Applied Biosciences) mass spectrometer. 3,5-dimethoxy-4-hydroxycinnamic acid was used as the matrix.

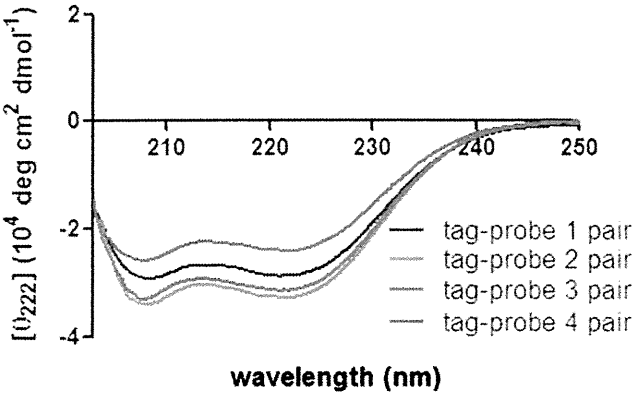

FIGURE 16 CD spectra of tag-probe pairs at 24°C in 50 m*M* Tris-HCl buffer (pH7.2, 100 m*M* NaCl): [tag-probe pair] = 1 μM. Tag-probe peptide **1** pair (blue), tag-probe peptide **2** pair (green), tag-probe peptide **3** pair (red) and tag-probe peptide **4** pair (magenta).

Peptide Synthesis

Probe peptides **1-5** were synthesized by the Fmoc-based solid-phase method.[26] The tag peptide was prepared previously.[20] All peptides were purified by RP-HPLC and identified by MALDI-TOF-MS. Fmoc-protected amino acids and reagents for peptide synthesis were purchased from Novabiochem, Kokusan Chemical Co., Ltd. and Watanabe Chemical Industries, Ltd. Fmoc-Dap(NBD)-OH was synthesized as previously reported.[30] The probe peptides **1-5** were synthesized using NovaSyn TGR resin on a 0.1 mmol scale. All peptides were synthesized by stepwise elongation techniques of Fmoc-protected amino acids on the resin. The coupling reactions were performed using 5.0 equiv. of Fmoc-protected amino acid, 5.0 equiv. of diiopropylcarbodiimide (DIPCI) and 5.0 equiv. of 1-hydroxybenzotriazole monohydrate (HOBt · H_2O) in DMF (5.0 mL). N-Terminal amino groups of the probe peptides **1-3** were chloroacetylated with chloroacetic acid, DIPCI and HOBt (5.0 equiv. each) in DMF (5.0 mL). N-Terminal amino groups of the probe peptides **4** and **5** were acetylated with acetic anhydride-DMF (1:4, v/v) (5.0 mL). In the synthesis of the probe peptide **5**, Fmoc-Lys(Mtt)-OH (Mtt = 4-methyltrityl) was coupled as the C-terminal Fmoc-protected amino acid. After construction of the protected peptide **5** resin and N-terminal acetylation, the peptide **5** resin was treated by dichloromethane-triisopropylsilane-TFA (94:5:1, v/v) (2.0 mL) for 1 min, and this treatment was repeated 11 times,[31] followed by N^{ε}-chloroacetylation with chloroacetic acid, DIPCI and HOBt (5.0 equiv. each) in DMF (5.0 mL). Cleavage and side chain deprotection of the probe peptides **1-5** was carried out with 10 mL of TFA in the presence of 0.25 mL of *m*-cresol, 0.75 mL of thioanisole, and 0.75 mL of 1,2-ethanedithiol as scavenger, by stirring for 1.5 h. After filtra-

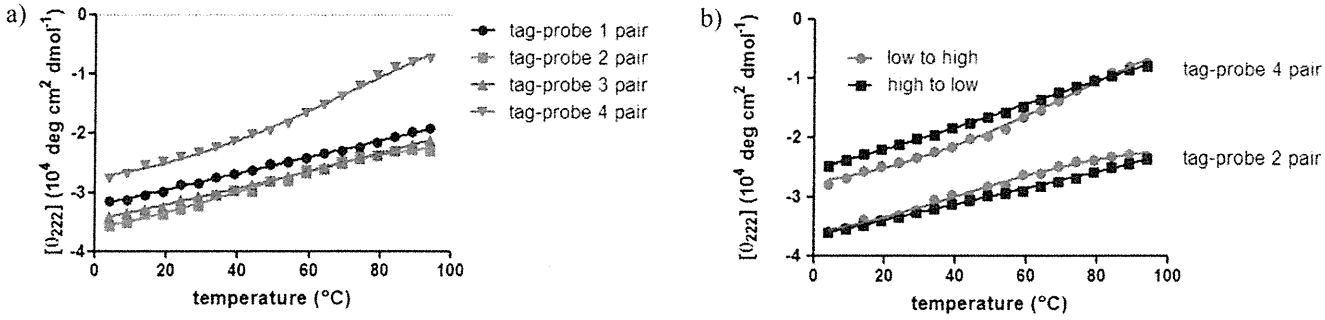

FIGURE 17 (a) Change of values of $[\theta]$ at 222 nm of tag-probe pairs from 4°C to 94°C in 50 m*M* Tris-HCl buffer (pH 7.2, 100 m*M* NaCl): [tag-probe pair] = 1 μM. Tag-probe **1** pair (blue), tag-probe **2** pair (green), tag-probe **3** pair (red) and tag-probe **4** pair (magenta). (b) Change of values of $[\theta]$ at 222 nm of tag-probe **2** and **4** pairs from 4°C to 94°C (low to high) (red) and from 94°C to 4°C (high to low) (blue) in 50 m*M* Tris-HCl buffer (pH 7.2, 100 m*M* NaCl).

tion, the reaction mixture was concentrated under reduced condition, and crude peptides were precipitated in cooled diethyl ether. All crude peptides were purified by RP-HPLC (column, YMC-Pack ODS-A, 10ϕ × 250 mm). The HPLC solvents employed were water containing 0.1% TFA (solvent A) and acetonitrile containing 0.1% TFA (solvent B). The probe peptides **1-5** was purified using a 23%–38% linear gradient of solvent B over 30 min. All purified peptides were identified by MALDI-TOF-MS. All peptides were obtained as TFA salts after lyophilization. Probe peptide **1**, yield 21%, *m/z* 2603.1, calcd 2603.5 $[M + H]^+$. Probe peptide **2**, yield 18%, *m/z* 2661.1, calcd 2660.6 $[M + H]^+$. Probe peptide **3**, yield 23%, *m/z* 2717.1, calcd 2717.6 $[M + H]^+$. Probe peptide **4**, yield 26%, *m/z* 2627.0, calcd 2626.6 $[M + H]^+$. Probe peptide **5**, yield 7%, *m/z* 2773.8, calcd 2773.7 $[M + H]^+$.

Crosslinking Reaction

The probe peptide (16 nmol) and tag peptide (16 nmol) were dissolved in 50 m*M* HEPES buffer, pH 7.2 containing 100 m*M* NaCl (16 mL), and incubated at room temperature in an N_2 atmosphere. At intervals (0, 1, 5, 10, 15, 20, and 30 min), an aliquot (1.6 mL) was sampled and 10% aqueous AcOH (0.4 mL) was added to the aliquot. The reaction was traced by HPLC using a 20%–50% linear gradient of solvent B over 30 min. HPLC peaks of the starting compounds and the generated products were identified by MALDI-TOF-MS: tag-probe peptide **1**, *m/z* 7880.4, calcd 7877.2 $[M + H]^+$. Tag-probe peptide **2**, *m/z* 7935.7, calcd 7934.2 $[M + H]^+$. Tag-probe peptide **3**, *m/z* 7993.8, calcd 7991.3 $[M + H]^+$. The amounts of the starting compounds and the generated products were quantified from the peak areas.

Fluorescence Titration Analysis

Fluorescence spectra were recorded on a JASCO FP-750 spectrometer using a quartz cell. A stock solution of the probe peptide was diluted with 50 m*M* HEPES buffer solution (pH 7.2, 100 m*M* NaCl) to prepare the solution with a final concentration (0.5 μM). The corresponding tag peptide solution was added dropwise to a 0.5 μM of the probe peptide solution and the fluorescence spectra (λ_{ex} = 456 nm) were measured at 25°C. An average value of three measurements was plotted as each point. Fluorescent titration curves (λ_{em} = 537 nm for probe **1** and **2**, 535 nm for probe **3**, and 534 nm for probe **4** and **5**) were analyzed with a nonlinear least-squares curve-fitting method to evaluate K_d values. For measurements of thermal denaturation, fluorescence spectra were recorded every 10°C from 4°C to 100°C after 10-min incubation of tag-probe pairs at each temperature. For measurements in thermal changes from high to low temperature, after 1-h incubation of tag-probe pairs at 100°C, fluorescence spectra were recorded every 10°C until 4°C. Tm values were estimated by a nonlinear least-squares curve-fitting method using GraphPad Prism 5 (MDF Co., Ltd.).

Fluorescence Job's Titration

The fluorescent intensity at 505 nm was recorded on a JASCO FP-750 spectrometer using a quartz cell in 50 m*M* HEPES buffer (pH 7.2, 100 m*M* NaCl) at 25°C. The total concentration of the probe peptide and the tag peptide was fixed at 1.0 μM. The concentrations of the tag peptide were 0, 0.2, 0.4, 0.5, 0.6, 0.8, and 1.0 μM. This fluorescence Job's titration experiment clearly indicates that the probe peptide binds to the tag peptide in a 1:1 stoichiometry.

CD Study

CD were recorded on a J-720WI spectropolarimeter using a quartz cell with 0.1 cm pathlength at 25°C. The stock solutions of tag-probe complexes were prepared and diluted with 50 m*M* Tris-HCl buffer solution (pH 7.2, 100 m*M* NaCl) to

prepare the solutions of a final concentration (1.0 μM). Each spectrum shows an average value of three measurements. For measurements of thermal denaturation, CD spectra were recorded every 5°C from 4°C to 94°C after 10-min incubation of tag-probe pairs at each temperature. For measurements in thermal changes from high to low temperature, after 1-h incubation of tag-probe pairs at 94°C, CD spectra were recorded every 5°C until 4°C.

The authors deeply thank Prof. K. Akiyoshi (Tokyo Medical and Dental Univ.) for allowing access to a CD spectropolarimeter.

REFERENCES

1. Terpe, K. Appl Microbiol Biotechnol 2003, 60, 523–533.
2. Hedhammar, M.; Gräslund, T.; Hober, S. Chem Eng Technol 2005, 28, 1315–1325.
3. Guignet, E. G.; Hovius, R.; Vogel, H. Nat Biotechnol 2004, 22, 440–444.
4. Goldsmith, C. R.; Jaworski, J.; Sheng, M.; Lippard, S. J. J Am Chem Soc 2006, 128, 418–419.
5. Hauser, C. T.; Tsien, R. Y. Proc Natl Acad Sci USA 2007, 104, 3693–3697.
6. Griffin, B. A.; Adams, S. R.; Tsien, R. Y. Science 1998, 281, 269–272.
7. Gaietta, G.; Deerinck, T. J.; Adams, S. R.; Bouwer, J.; Tour, O.; Laird, D. W.; Sosinsky, G. E.; Tsien, R. Y.; Ellisman, M. H. Science 2002, 296, 503–507.
8. Marks, K. M.; Rosinov, M.; Nolan, G. P. Chem Biol 2004, 11, 347–356.
9. Ojida, A.; Honda, K.; Shinmi, D.; Kiyonaka, S.; Mori, Y.; Hamachi, I. J Am Chem Soc 2006, 128, 10452–10459.
10. Chen, I.; Choi, Y.-A.; Ting, A. Y. J Am Chem Soc 2007, 129, 6619–6625.
11. O'Hare, H. M.; Johnsson, K.; Gautier, A. Curr Opin Struct Biol 2007, 17, 488–494.
12. Keppler, A.; Gendreizig, S.; Gronemeyer, T.; Pick, H.; Johnsson, K. Nat Biotechnol 2003, 21, 86–89.
13. Gautier, A.; Juillerat, A.; Heinis, C.; Correa, I. R., Jr.; Kindermann, M.; Beaufils, F.; Johnsson, K. Chem Biol 2008, 15, 128–136.
14. Yin, J.; Liu, F.; Li, X.; Walsh, C. T. J Am Chem Soc 2004, 126, 7754–7755.
15. Los, G. V.; Darzins, A.; Karassina, N.; Zimprich, C.; Learish, R.; McDougall, M. G.; Encell, L. P.; Friedman-Ohana, R.; Wood, M.; Vidurgiris, G.; Zimmerman, K.; Otto, P.; Klaubert, D. H.; Wood, K. V. Promega Cell Notes 2005, 11, 2–6.
16. Tripet, B.; Yu, L.; Bautista D. L.; Wong, W. Y.; Irvin, R. T.; Hodges, R. S. Protein Eng 1996, 9, 1029–1042.
17. Zhang, K.; Diehl, M. R.; Tirrell, D. A. J Am Chem Soc 2005, 127, 10136–10137.
18. Obataya, I.; Sakamoto, S.; Ueno, A.; Mihara, H. Biopolymers 2001, 59, 65–71.
19. Yadav, M. K.; Redman, J. E.; Leman, L. J.; Alvarez-Gutie'rrez, J. M.; Zhang, Y.; Stout, C. D.; Ghadiri, M. R. Biochemistry 2005, 44, 9723–9732.
20. Tsutsumi, H.; Nomura, W.; Abe, S.; Mino, T.; Masuda, A.; Ohashi, N.; Tanaka, T.; Ohba, K.; Yamamoto, N.; Akiyoshi, K.; Tamamura, H. Angew Chem Int Ed 2009, 48, 9164–9166.
21. Lovejoy, B.; Choe, S.; Cascio, D.; McRorie, D. K.; DeGrado, W. F.; Eisenberg, D. Science 1993, 259, 1288–1293.
22. Kuwabara, T.; Nakamura, A.; Ueno, A.; Toda, F. J Phys Chem 1994, 98, 6297–6303.
23. Ward, S. G.; Westwick, J. Biochem J 1998, 333, 457–470.
24. Tamamura, H.; Tsutsumi, H.; Nomura, W.; Tanaka, T.; Fujii, N. Exp Opin Drug Disc 2008, 3, 1155–1166.
25. Nomura, W.; Tanabe, Y.; Tsutsumi, H.; Tanaka, T.; Ohba, K.; Yamamoto, N.; Tamamura, H. Bioconjugate Chem 2008, 19, 1917–1920.
26. Chan, W. C.; White, P. D. In Fmoc Solid Phase Peptide Synthesis: A Practical Approach; Chan, W. C.; White, P. D., Eds.; Oxford University Press: New York, 2000; pp 41–76.
27. Dawson, P. E.; Muir, T.W.; Clark-Lewis, I.; Kent, S. B. H. Science 1994, 266, 776–779.
28. Muir, T. W.; Kent, S. B. H. Annu Rev Biochem 2000, 69, 923–960.
29. Nonaka, H.; Tsukiji, S.; Ojida, A.; Hamachi, I. J Am Chem Soc 2007, 129, 15777–15779.
30. Kamoto, M.; Umezawa, N.; Kato, N.; Higuchi, T. Chem Eur J 2008, 14, 8004–8012.
31. Bourel, L.; Carion, O.; Gras-Masse, H.; Melnyk, O. J Peptide Sci 2000, 6, 264–270.